

14 Design and Performance of Duct Acoustic Treatment

2-11
1/1/50
N92-14783

Lead authors

R. E. Motsinger
General Electric Co.
Cincinnati, Ohio

R. E. Kraft
General Electric Co.
Cincinnati, Ohio

GE 100 602

Orientation

This chapter discusses the procedure for designing acoustic treatment panels used to line the walls of aircraft engine ducts and for estimating the resulting suppression of turbofan engine duct noise. This procedure is intended to be used for estimating noise suppression of existing designs or for designing new acoustic treatment panels and duct configurations to achieve desired suppression levels.

Federal and local government regulations limit the level of noise that may radiate from commercial and private aircraft. Some airports impose even more severe limits, such as the Washington International Airport at night. Noise certification levels of aircraft, which are the starting point for determining the required noise suppression, are discussed in the chapter on flyover noise measurement and prediction.

In general, the noise levels generated by the source mechanisms of turbomachinery used in turbofan-powered aircraft are higher than allowed by the regulated limits. Suppression within the engine ducts, both inlet and exhaust, is necessary to meet certification levels. These noise sources normally consist of the turbofan, compressor, turbine, and combustor.

The amount of required noise suppression often establishes the length of ducting requiring treatment. Because duct lengths should be as short as possible to control weight, the designer must be concerned that the source level of each engine component is appropriately determined.

To estimate the engine contribution to aircraft flyover noise, information is needed on both suppression and the effect of the suppression on the far-field radiation pattern. Experience has shown that the required noise suppression can be predicted

reasonably well for the inlet, but the suppression required for each aft end component (fan duct, core nozzle) is not easily established.

The problem in the aft end stems from difficulty in unambiguously separating fan, turbine, jet, and combustion components contributing to the overall radiated level. The measurement of suppression of a treatment design for one of these components is difficult, particularly if the contribution of that component is 10 dB or more below the combined level of the other sources. In this case, the small decrease in the overall level of noise due to the increased suppression of the component cannot be distinguished from experimental error in the measurement.

In addition, it is important that the type of acoustic treatment panels selected have the appropriate suppression characteristics as a function of frequency. The treatment is usually designed to preferentially suppress the noise generated in those frequencies that contribute most to the aircraft noise as measured in noise certification units (perceived noise level).

Design Approach

Perspectives on Treatment Design

The panel design and associated suppression depend on the noise source characteristics defined by acoustic modes propagating within the duct, which acts as a wave guide. There are two distinct regimes, one in which the wavelength is large relative to the duct opening and the other in which it is small. Rigorous analytical techniques are necessary in the former, but ray acoustics or empirical methods are usually adequate in the latter. For the "gray" area, where large- and small-wavelength regimes overlap, a combination of the two approaches is required.

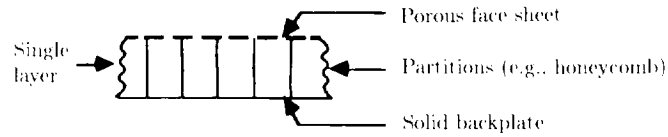
The key design parameter is the acoustic impedance of the treatment panel. The impedance is comprised of a real part, the resistance, and an imaginary part, the reactance. In practice, analytical estimation of suppression as a function of the treatment acoustic impedance forms the basis for typical designs. The results of this approach set the acoustic impedance design criteria for the treatment panels in new applications or improve performance of existing designs.

Because of limitations to the current state of the art of rigorous discrete-frequency duct propagation theory, the analytical approach is seasoned with engineering data to establish a priori estimates of the likely performance of treatment designs for new applications. Specifically, suppression is parametrically analyzed to establish the values of panel resistance and reactance that provide the closest approach to maximum suppression for the assumed engine source characteristics, within practical constraints dictated by other considerations. This analysis is performed over the frequency range of concern to establish the treatment acoustic impedance design criteria for the engine component.

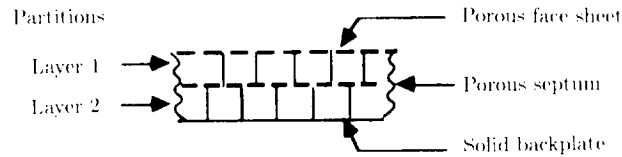
The next step is to design the treatment panel to match as closely as possible the desired impedance for each frequency band of concern. Depending on the range of frequency over which suppression is required, the type of treatment is then chosen: single degree of freedom (SDOF), two degree of freedom (2DOF), or bulk absorber.

The SDOF design, shown in figure 1(a), consists of a single-layer sandwich construction with a solid backplate, porous face sheet, and cellular separator such as honeycomb. The 2DOF design, shown in figure 1(b), adds a second layer (double-layer sandwich), with a porous septum sheet, or midsheet. This concept could be

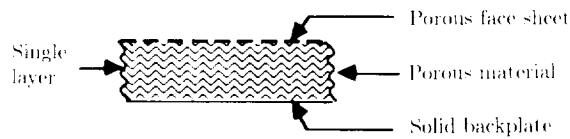
extended to multiple layers. The bulk absorber, shown in figure 1(c), has a single-layer construction in which a fibrous mat fills the panel between the porous face sheet and solid backplate.



(a) Single degree of freedom (SDOF).



(b) Two degree of freedom (2DOF).



(c) Bulk absorber.

Figure 1. Conventional aircraft engine treatment panel designs.

Of the three design types, the SDOF type is effective over the narrowest range of frequencies and must be tuned to the frequency band containing the single fan tone of greatest concern. The useful bandwidth of SDOF treatment is about one octave. The 2DOF type has a wider bandwidth, being most effective for two adjacent harmonics of fan blade-passage frequency (BPF). With careful design, the useful bandwidth of 2DOF treatment can be extended to cover the BPF and its next two harmonics (about two octaves). This is generally sufficient for turbofan engine applications. The bulk absorber has the widest bandwidth, extending over three octaves in the range of concern if the panel is made sufficiently deep to be effective at the lowest frequency. Its performance at the higher frequencies then depends on the selection of fiber diameter and material density. Bulk absorber treatment has not been used in aircraft engines in commercial service because of structural design difficulties.

Note that the SDOF and 2DOF treatments are resonator panels, and their acoustic properties strongly depend on the damping that the resistance of the face sheet and midsheet provides; the acoustic properties can be either linear or nonlinear. The damping resistance of nonlinear liner face sheets and septum sheets varies with the amplitude of the acoustic wave incident on the liner, whereas the resistance of

linear face sheets and septum sheets is independent of the incident wave amplitude, at least over the range of sound pressure levels (SPL) experienced in practice. Thus, the resistance of a nonlinear treatment panel may vary along the length of the duct, as the wave amplitude is suppressed, and this variation affects its acoustic performance.

Ordinary perforate materials, typically with 1/32- to 1/16-inch-diameter holes, are in the nonlinear category. Wire-mesh materials and bulk absorbers are in the linear category except at extremely high SPL.

Generally, a more controlled treatment panel design can be obtained by using linear materials, which, to some extent, makes the treatment impedance independent of engine power setting. Since the source characteristics are known to change with engine power setting, attempting to maintain a constant treatment impedance is an oversimplification of the design problem. Conceivably, with highly sophisticated techniques, a nonlinear material could be designed with a variable impedance that used changing SPL to track optimum impedance values better than a linear material, but such an approach is beyond the scope of this discussion.

Available Design Approaches

Three design approaches are available to the acoustic engineer confronted with an engine noise suppression problem: theoretical, semiempirical, or empirical. Figure 2 illustrates graphically the acoustic treatment design approaches. The purpose of this chapter is to provide guidance to the engineer in selecting and implementing a treatment design method.

Ideal Theoretical Design Procedures

The theoretical design procedures discussed in the previous chapter represent the ideal approach for the analysis of duct acoustic propagation and radiation. These methods require knowledge of, or at least an assumption about, the source characteristics. At each problem frequency, the amplitudes and relative phases of the duct modes that are excited by the source (e.g., Tyler-Sofrin modes), or equivalent information in terms of acoustic pressure profiles, must be known for input into the analysis.

Elaborate experimental methods have been developed to measure modal content on vehicles that present unusually difficult problem tones. Successful suppression of these tones requires a closely tailored treatment design. Such theoretical design procedures represent current state of the art and have been applied in practice when the number of modes that are excited is modest. This problem arises sufficiently often to justify the significant effort required to exercise that capability.

Semiempirical and Empirical Approaches

When there is little information about the source modal characteristics, either because the particular turbomachinery is still in the early design stage and component test data are not available or because the number of duct modes carrying energy is very large (typical of high-bypass-ratio turbofan inlets), assumptions about the source characteristics usually must be made. The analytical result then becomes dependent on the modal content assumption, and experience must be a factor in providing a "best guess" assumption. To the extent that the input source characteristics are uncertain, the rigorous analysis becomes somewhat semiempirical.

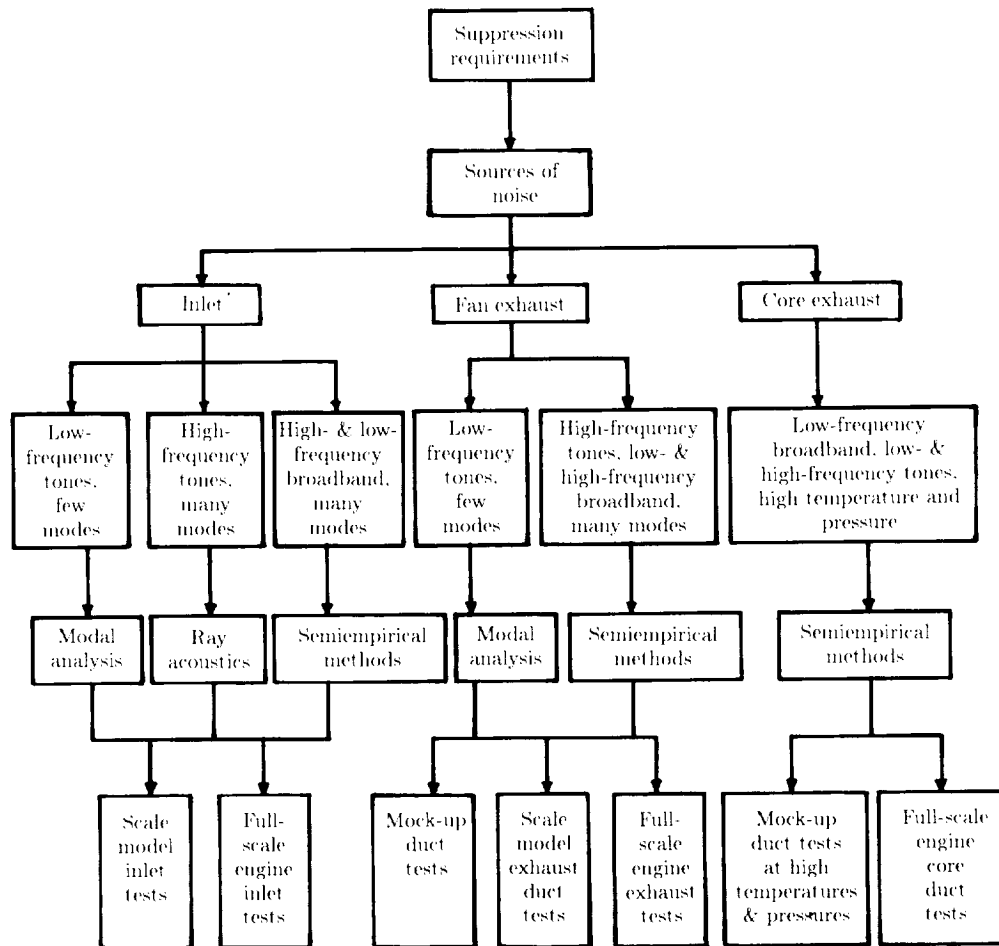


Figure 2. Schematic of engine treatment design approaches.

Progress is being made in turbomachinery source-prediction methods so that, again with experience, this prediction could reduce the uncertainty of the semiempirical procedure. On the other hand, besides the possible uncertainty about the source, the actual conditions within engine ducts often depart significantly from the ideal. Interruptions in the treatment both circumferentially and axially, axial variations in the duct height, duct curvature, and other such departures from the ideal introduce the need to augment the theoretical approach with experimental data.

In the early years of development of acoustic treatment design for turbofan engine ducts, theoretical methods were not generally available nor sufficiently complete to permit designs by other than the purely empirical approach. The empirical approach usually consists of laboratory measurement of noise suppression, or insertion loss, when acoustic treatment is applied to the walls of a duct built to simulate the geometry of the engine duct.

The insertion loss experimental method compares the noise levels measured for a hard-walled, untreated duct with the levels measured after treatment panels have been inserted. Choices of treatment designs used for these tests are based on engineering experience, and because of the cost, the test series is seldom sufficiently exhaustive to ensure that the optimum design has been achieved. Examples of such test facilities are discussed in the subsequent section entitled "Testing for Treatment Design and Performance Measurement."

For either inlet or exhaust ducts, some of the pure empiricism can be removed by conducting an experimental test program in which SDOF treatment designs are employed. During a series of insertion loss tests the treatment panel depth and face-sheet resistance are systematically varied. The variation of panel depth controls variation of the treatment reactance, while the face-sheet resistance is varied by means of porosity if it is a perforate, or Rayl number if it is a mesh. The measured suppression can be plotted in the impedance plane, where the impedance of the panels tested has been obtained using existing methods for predicting or measuring panel impedance. Contour plots of isosuppression at each frequency then provide data on suppression in terms of impedance. Since the wall impedance is assumed to be the key parameter determining the suppression performance of the treatment panel, the isosuppression plots can be used in a semiempirical manner to predict the suppression of more complicated 2DOF or bulk absorber panels at each frequency, when the impedance for such panels is obtained by either prediction or measurement in the laboratory.

Another example of a semiempirical approach is to make geometric acoustic approximations in the analytical model used to represent the propagating sound field. For the inlet at blade-passage frequency and higher (ratio of duct diameter to wavelength greater than 10), suppression and far-field directivity of broadband noise can be closely estimated by means of simple ray acoustics, assuming equal energy distribution among the propagating modes. This semiempirical method is not adequate, however, when the noise is in a strong tone which is carried by relatively few modes excited by a source characteristic such as a vane-blade interaction. Fortunately, these exceptional cases are amenable to the rigorous analytical methods described in the previous chapter.

Design Approach Advantages and Disadvantages

The principal differences among the three approaches, and their relative advantages and disadvantages, are

1. The empirical approach requires extensive testing, which is not only time-consuming and expensive but also may not give adequate representation, or mock-up, of the conditions in the engine application. Laboratory tests can give ballpark designs, but actual engine tests are, ultimately, the most reliable way of arriving at an answer. If the design is marginal because a particular problem is unusually severe, a number of candidate designs may need to be tested.
2. The semiempirical approach by its nature entails some theoretical basis to provide coherence and understanding to the meaning of experimental data. Thus, the amount of testing required is reduced in scope and the time needed is significantly shortened. The main problem is to identify the analytical model that can be used with a limited data base to reach the objective.

3. The rigorous theoretical approach is most useful in providing understanding of the basic phenomena involved in the problem. In most cases, the rigorous model is a simplification or idealization of the actual conditions of the design application. Nevertheless, particularly when working with an actual engine development program, the theoretical approach provides such insight into cause and effect that the shortcomings of the model can be overshadowed by the gain in knowledge and understanding achieved.

Fundamentals of Duct Liner Technology

Acoustic Impedance Design Criteria

Acoustic impedance is defined as the ratio of acoustic pressure to acoustic velocity at a point on the surface of the panel and is given by the complex number

$$Z = \frac{p}{v} = R + iX \quad (1)$$

where

Z impedance, cgs rayls ($\text{g}/\text{cm}^2\text{-sec}$)

p acoustic pressure, dynes/ cm^2

v acoustic velocity, cm/sec

R acoustic resistance, cgs rayls

X acoustic reactance, cgs rayls

$i = \sqrt{-1}$

The convention used in this chapter for time dependence of the wave solution of acoustic pressure and velocity in the duct is $e^{+i\omega t}$ (where ω is circular frequency and t is time). This leads to a positive sign for the imaginary term in the impedance, which is the usual convention. Choosing the $e^{-i\omega t}$ sign convention requires taking the complex conjugate in the definition of impedance. Further discussion of impedance (and its inverse, admittance) is given in reference 1, pp. 21-24; units and conversion factors are defined in reference 2. One of the first discussions of the impedance properties of treatment panels used in aircraft engine ducts is presented in reference 3.

Point-reacting treatment is used in aircraft engines and is the basis for the methods discussed in this chapter. To be point-reactive, the treatment panel must contain partitions that prevent propagation of the sound laterally within the panel. The point-reacting condition (which is also referred to as locally reacting) is required for the concept of impedance to be valid as a design parameter. In a non-point-reacting panel, the impedance at a point depends on the wave motion within the panel in an extended region around the point, and analysis of the design and performance of such panels must include the lateral propagation inside the panel.

As a rule of thumb, the axial extent of the partitions for resonators (SDOF, 2DOF) should be less than the depth of the panel, and partitions to block both axial

and circumferential internal propagation are desirable. In bulk absorbers, partitions with 2-inch to 4-inch axial spacing have typically been used for panels nominally 1-inch thick.

The value of impedance that provides the maximum sound absorption at a given frequency depends on the acoustic mode or ray angle of the propagating sound wave. The dependence is discussed for illustration briefly in the following paragraphs and in more detail in an elementary but clear way in reference 4, pp. 98-140. Reference 4 implicitly reveals the value of normalizing the impedance by the characteristic impedance of air ρc , such that

$$\frac{Z}{\rho c} = \zeta = \theta + i\chi = \frac{R}{\rho c} + \frac{iX}{\rho c} \quad (2)$$

where

- ζ = $Z/\rho c$, the (nondimensional) impedance ratio
- θ = $R/\rho c$, the (nondimensional) resistance ratio
- χ = $X/\rho c$, the (nondimensional) reactance ratio
- ρ = density of the medium (air), g/cm³
- c = speed of sound in the medium, cm/sec

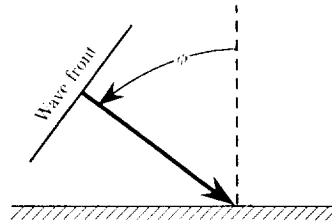
One way of analyzing acoustic propagation in an idealized two-dimensional wave guide is to consider each wave to be the superposition of a series of plane waves, where each plane wave strikes the wall at a different angle and then ricochets back and forth down the duct. Reference 5, pp. 493-495, shows that in a hard-walled duct this plane-wave solution is equivalent to an acoustic mode propagating in the duct and that only certain angles of incidence to the wall (the characteristic duct modes) are allowed. This plane-wave analogy can be used to lend physical insight into the absorption process in ducts.

For the idealized case of a plane wave incident on a flat surface, the fraction of incident energy absorbed by the treatment panel is

$$\alpha = \frac{4\theta \cos \phi}{(1 + \theta \cos \phi)^2 + (\chi \cos \phi)^2} \quad (3)$$

where

- α = absorption coefficient
- ϕ = angle between the normal to the wave front and the normal to the panel, as shown in the sketch



The normal-incidence absorption coefficient is the value of α when $\phi = 0$.

Equation (3) is based on the plane-wave solution to the wave equation for a reflection at a surface, assuming a semi-infinite region above the surface. This model is valid for propagation in a duct in the short wavelength (ray acoustic) limit so long as ϕ is not close to 90° . In that case, when the wave is propagating parallel to the wall, a modal analysis approach is required (see Cremer, ref. 6). For the plane-wave mode ($\phi = 90^\circ$) without airflow, Cremer's analysis yields the optimum impedance for ducts of rectangular cross section:

$$Z_{\text{opt}}/\rho c = (0.92 - 0.77i)\eta \quad (4)$$

or

$$R/\rho c = 0.92\eta \quad X/\rho c = -0.77\eta$$

where

$\eta = H/\lambda$, nondimensional frequency parameter

H height between duct walls, cm

λ wavelength of sound, cm

In contrast, the plane-wave surface reflection result indicates that the value of α is maximum when $X = 0$ and $R/\rho c = 1/\cos \phi$; that is, to obtain maximum absorption, the angle of incidence of the sound ray must be taken into account. In the event of many different ray angles, or propagating modes, the best choice of the value of R depends, then, on the amount of energy in each of the rays and on the relative attenuation rate introduced by the panel impedance selection.

Note that the plane-wave angle of incidence result for optimum modal impedance is an approximation to the exact result for a given mode. Determination of the exact optimum impedance requires solution of a complex transcendental equation derived from the duct impedance boundary condition (see the previous chapter).

If a single mode is dominant and giving trouble in the far field, the treatment may possibly be designed for it alone. The typical design problem is not that simple. Usually, there is a mix of modes with energy distributed among them in a manner that is generally unknown and, as experience to date has indicated, not easily measured. Thus an engineering assumption about the modal distribution must be introduced in order to attempt an analytical design approach. Failing an analytical approach, the designer must resort to laboratory mock-up duct testing, or even to engine testing.

The direct engine or mock-up duct testing approach has been often used, but results of laboratory mock-up duct tests for curved-duct fan reversers and engine tests for inlets suggest that a good engineering assumption for the analytical approach in these cases is to assume equal energy in all cut-on modes and random phasing among modes. At present, this provides a basis for semiempirical analytical determination of the best choices of R and X and estimation of the suppression losses caused by nonoptimum values.

In choosing the mock-up duct test approach, the designer must be aware that the source being used in laboratory testing may not closely simulate the actual engine source. Moreover, even if an engine is used as the treatment design testbed, the characteristics of certain tones produced in the presence of inflow distortion (such as

would be encountered with static engine ground testing) may be quite different from those produced in flight with cleaner inflow. When the equal energy and random phasing assumption holds, the mock-up duct procedure provides useful guidance in determining the effects of changes in duct geometry or treatment impedance, and engine static test results are improved by the provision of inlet turbulence control structures, as discussed subsequently.

Panel Configuration Design

In many cases, the desired resistance increases monotonically with frequency. Desired reactance is close to zero or even negative and becomes more negative with increasing frequency, as suggested by Cremer's (ref. 6) result (eq. (4)). These properties can be achieved over a limited range of frequency in the 2DOF construction. SDOF designs require a series of different treatment segments along the duct to achieve the same objective. Also, now that reasonably accurate impedance prediction is possible for bulk absorbers, it is understood that their previously known wide suppression bandwidth originates from inherently possessing a favorable variation of impedance (both R and X) as a function of frequency.

The properties of candidate panels and evaluations of their ability to achieve the impedance design criteria are summarized in the following sections.

Single-Degree-of-Freedom Liners

The SDOF panel (see fig. 1(a)) has a single-layer sandwich construction with a solid backplate, porous face sheet, and internal partitions as would be provided by a honeycomb. The face sheet can be a perforate with or without bonded wire mesh. The perforate is suitable for a limited range of power settings, for example, either for approach or for takeoff; if designed at one point, the other may be somewhat compromised. On the other hand, the wire mesh permits a uniform resistance property over a wide range of duct sound pressure levels and airflow velocities.

Linear face sheets maintain constant resistance with frequency because of the low-Reynolds-number viscous pressure drop for very fine screens. Nonlinear materials are effectively linearized by mean flow for typical duct Mach numbers, but may exhibit slight nonlinear resistance peaks near frequencies where the reactance approaches zero.

The reactance of single-layer panels follows a slightly modified cotangent curve, so that the optimum value can be obtained only at a single tuning frequency.

Two-Degree-of-Freedom Liners

The 2DOF panel (see fig. 1(b)) has a double-layer sandwich construction with a solid backplate, porous septum, and porous face sheet. Internal partitions such as honeycomb provide the spacing for the two layers. As with SDOF panels, the face sheet can be a perforate with or without bonded wire mesh. Even with the use of perforate only, linear properties can be approached because the septum can be made to control most of the effective acoustic resistance of the panel.

To obtain a linear property for the panel as a whole, the septum should be nearly linear. Septum linearity can be approached by using a perforate with such small holes (in the range of 5 to 10 mils) that the acoustic velocities induce only laminar orifice

flow. The closest approach to linearity identified to date, other than a bulk absorber, is to use a septum of wire mesh alone; such construction is available commercially.

The introduction of the septum has these important benefits: (1) the resistance of the panel surface is controlled by the septum rather than by the face sheet and thus the panel properties are essentially independent of duct flow effects; (2) the resistance and reactance can be tailored to approach the desired design values over a moderate range of frequencies. To achieve this benefit, the face-sheet resistance must be small. Figure 3 illustrates the degree of control of the panel properties obtainable.

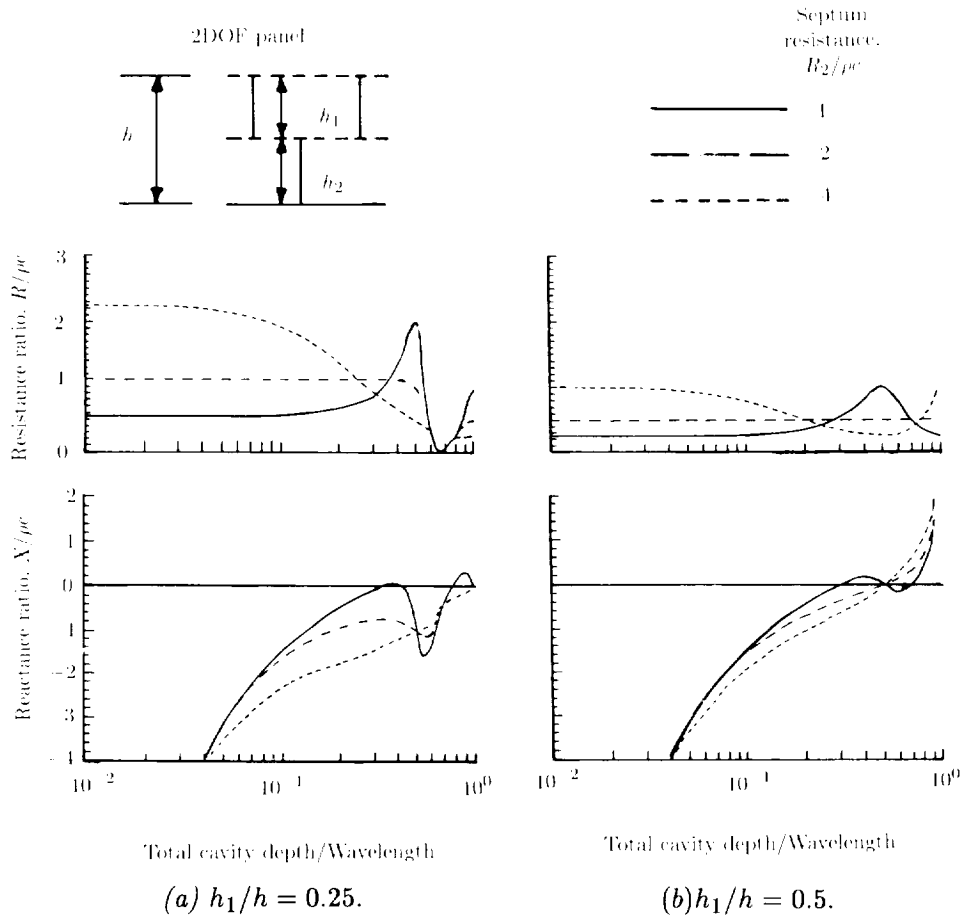


Figure 3. Effect of variation of septum placement and resistance on impedance of 2DOF treatment, for face-sheet resistance of zero.

Bulk Absorber

A bulk absorber panel (see fig. 1(c)) usually consists of a single-layer construction with solid backplate and porous face sheet of negligible resistance (approximately 30-percent porosity or higher). The cavity is filled with a fibrous mat having very small air passages so that the airflow through the mat (acoustic velocity excitation) is of sufficiently low Reynolds number to be laminar throughout.

The introduction of the bulk absorber into the cavity has the same advantages as the introduction of the septum in 2DOF panels. The difference between the two is that the internal resistance of the 2DOF panel is "lumped," while that of the bulk absorber is distributed continuously over the panel depth. The 2DOF design can be tailored by varying the resistance of the septum and its location. The bulk absorber design (assuming homogeneous material) can be tailored by varying the amount of internal flow resistance (density of mat, fiber diameter, etc.).

Desired minimum tuning frequencies can be achieved with slightly thinner panel depths for bulk absorbers than for resonators, because the effective speed of sound is reduced by viscosity and heat transfer to and from the mat. The distributed resistance of bulk absorbers damps all multiples of half-wave antiresonances, whereas the 2DOF panel damps only the first one. Thus, the bulk absorber can absorb sound effectively at all frequencies above the first quarter-wave resonance, but the 2DOF panel performs well only for the range from the fan fundamental to the third harmonic.

Impedance Models

A comprehensive summary of analytical models for predicting impedance of treatment materials is given in reference 7. This report includes methods for point-reacting and distributed-reacting materials and for single- and multi-layered panels. The following discussion is specialized for the specific types of liners described in the preceding section, with emphasis on the kinds of liners that have been widely used in commercial engine ducts.

Design Parameters

By examining the mathematical models for treatment impedance for each panel type, we can readily identify the key parameters that relate the impedance to the physical construction. These physical parameters are denoted in figure 4.

The general formulas for each panel type are as follows:

For single-degree-of-freedom panels (fig. 4(a)),

$$\frac{Z}{\rho c} = \frac{R}{\rho c} + i \left(\frac{X_m}{\rho c} + \frac{X_c}{\rho c} \right) \quad (5)$$

where

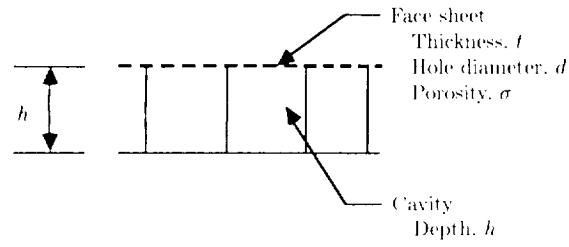
$R/\rho c$ face-sheet resistance

$X_m/\rho c$ face-sheet mass reactance

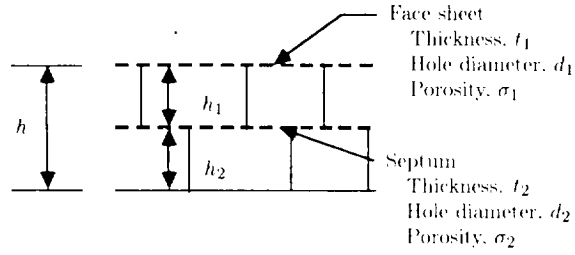
$X_c/\rho c$ cavity reactance, equal to $-\cot(kh)$

h cavity depth, cm

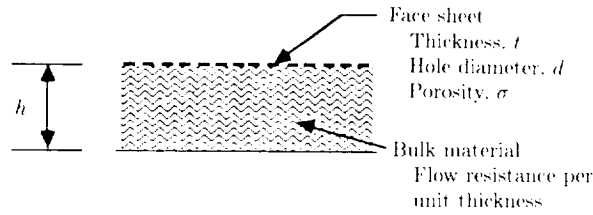
k wave number, equal to ω/c , cm^{-1}



(a) Single degree of freedom.



(b) Two degree of freedom.



(c) Bulk absorber.

Figure 4. Treatment panel design parameters.

For two-degree-of-freedom panels (fig. 4(b)),

$$\frac{Z}{\rho c} = \frac{Z_1}{\rho c} + \frac{\frac{Z_2 \cos(kh_1) \sin(kh_2)}{\rho c} - i \cot(kh)}{1 + i \frac{Z_2 \sin(kh_1) \sin(kh_2)}{\rho c \sin(kh)}} \quad (6)$$

where subscript 1 denotes the face sheet's impedance, resistance, and mass reactance and subscript 2 denotes the septum's; thus

$$\frac{Z_1}{\rho c} = \frac{R_1}{\rho c} + i \frac{X_{m1}}{\rho c}$$

$$\frac{Z_2}{\rho c} = \frac{R_2}{\rho c} + i \frac{X_{m2}}{\rho c}$$

For bulk absorber panels (fig. 4(c)),

$$\frac{Z}{\rho c} = \frac{Z_B}{\rho c} + \xi \coth(\gamma h) \quad (7)$$

where subscript B denotes the face-sheet impedance, resistance, and mass reactance, that is,

$$\frac{Z_B}{\rho c} = \frac{R_B}{\rho c} + i \frac{X_B}{\rho c}$$

and where

- ξ characteristic impedance ratio of impedance of the bulk absorber to that of air
- γ propagation coefficient (wave number) in the bulk absorber

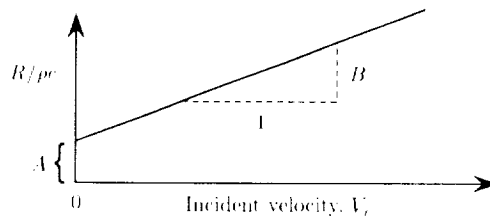
The bulk absorber formulas have been adapted from reference 8. Expressions to calculate each of the parameters in these equations are given in the following discussion.

A more fundamental analytical model for bulk absorber panel impedance that should be pursued further is given in reference 9. That model, if modified to use dc flow resistance properties as input, could substantially improve the prediction of bulk absorber impedance.

Resistance: For the face sheet in the absence of grazing flow and for septum materials, the resistance term can be determined by the expression

$$\frac{R}{\rho c} = A + BV_i \quad (8)$$

where A and B are determined experimentally by dc flow resistance measurements and V_i is the velocity incident on the sample. The velocity can be taken as either the dc flow velocity or the root-mean-square of the fluctuating acoustic velocity incident on the sample. Making this identification is what relates the dc flow resistance measurement to acoustic resistance.



When the measurements of dc flow resistance are plotted versus incident velocity on a linear scale, the results can be described by a linear relationship (see ref. 10). The value of A is the linear component of the resistance, while B is the nonlinear

component, since the velocity-dependent term is what makes the resistance a function of the amplitude of the incident wave. In general, wire-mesh materials have both the A and the B component, while ordinary perforate materials have a significant value only for the B component.

For perforate materials, parameters determining the A and B terms can be identified from simple fluid mechanics, considering the energy loss mechanism to be caused by the pressure differential across the sample. Figure 5 illustrates the flow energy dissipation mechanisms comprising the resistance. The first term in equation (8) is the pressure loss inside the hole due to pipe-flow friction; the second term is dynamic head loss due to the turbulence associated with entrance and exit losses.

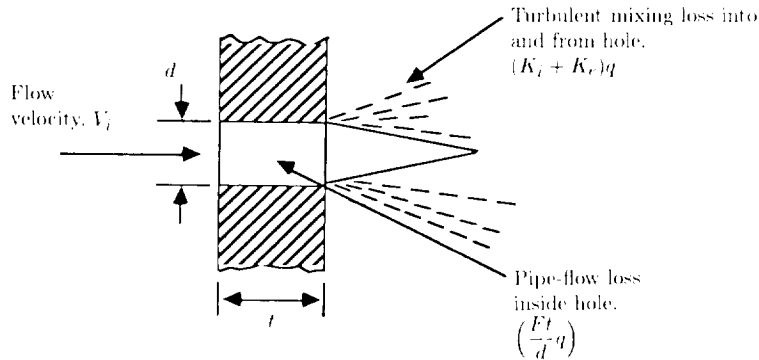


Figure 5. Flow mechanisms for dc flow resistance.

The first term is important when the diameter of the opening d is so small that the flow through the pore is laminar. This is the case for wire-mesh materials; for ordinary perforates, the flow in the hole is turbulent and the second term dominates. In the following analysis we express equation (8) in terms of acoustic resistance. This permits identification of the parameters that allow estimation of the effect of temperature and pressure on the material's resistance properties.

First, we note that for laminar flow, the friction factor is inversely proportional to Reynold's number N_{Re} :

$$F = \frac{a}{N_{Re}} = \frac{a\mu}{\rho V_h d} \quad (9)$$

where

- F friction factor for pipe flow
- V_h velocity in the orifice, cm/sec
- μ fluid dynamic viscosity, dynes-sec/cm²
- d hole diameter, cm
- ρ fluid density, g/cm³
- a dimensionless proportionality constant, equal to 64

The ratio of pressure loss to dynamic pressure of the fluid within the hole is given by

$$\frac{\Delta p}{q} = \frac{Ft}{d} + K_i + K_e \quad (10)$$

where

- Δp pressure loss, dynes/cm²
 q dynamic head, dynes/cm²
 t thickness of face sheet, cm
 K_i dimensionless entrance loss
 K_e dimensionless exit loss

For commercially available perforate materials, experience has shown that $K_i + K_e$ is approximately 1. The dynamic pressure in the orifice for incompressible flow is given by

$$q = \frac{1}{2}\rho V_h^2 \quad (11)$$

Note that this can be extended to compressible flow as in reference 11. The equivalent velocity through the vena contracta of the orifice is given by

$$V_h = \frac{V_i}{C_D\sigma} \quad (12)$$

where C_D is the dimensionless orifice discharge coefficient. A typical value of the discharge coefficient is $C_D \approx 0.76$. The porosity σ is given by

$$\sigma = \frac{n\pi d^2}{4} \quad (13)$$

where n is the number of holes per unit area.

Substituting equations (9), (11), and (12) into equation (10) and solving for $\Delta p/\rho c V_i$ results in

$$\frac{R}{\rho c} = \frac{\Delta p}{\rho c V_i} = \frac{a\mu t}{2\rho c(\sigma C_D)d^2} + \frac{K_i + K_e}{2c(\sigma C_D)^2} V_i \quad (14)$$

where we have inherently identified the dc flow velocity with the root-mean-square acoustic velocity. Comparing this result with equation (8), we obtain

$$A = \frac{a\mu t}{2\rho c(\sigma C_D)d^2} \quad (15)$$

$$B = \frac{K_i + K_e}{2c(\sigma C_D)^2} \quad (16)$$

Thus, A depends on both temperature (through c , μ , and ρ) and pressure of the air (through ρ) and B depends only on the temperature (through c). The values of a , C_D , and $K_i + K_e$ depend on the sheet material, whether wire mesh or simple perforate, and are most accurately determined from a dc flow resistance measurement of the actual material, which measures A and B directly.

Mass reactance: For the face-sheet and septum materials, the mass reactance term is determined by

$$\frac{X_m}{\rho c} = \frac{k(t + \epsilon d)}{\sigma} \quad (17)$$

where ϵ is the dimensionless end correction, which depends on the type of face-sheet or septum material. For perforates as in figure 5, early literature suggests $\epsilon = 0.85$; Ingard deduced a porosity effect (ref. 12):

$$\epsilon = 0.85 (1 - 0.7\sqrt{\sigma}) \quad (18)$$

Note that ϵ also depends on sound pressure level and grazing flow effects (as discussed subsequently). In the septum of 2DOF panels, equation (18) is applicable because there are no grazing flow effects and the sound pressure level at the septum is relatively small. When the perforate is used over a bulk absorber, the porosity should be relatively high (greater than 25 percent), so the face sheet is acoustically transparent. For that reason, little attention has been given to this case, but, to a first approximation, the resistance term for a perforate should be valid, and the end correction on mass reactance should be about 0.3.

Bulk absorber parameters: The ratio of the characteristic impedance of the bulk absorber to that of air is given by

$$\frac{Z_B}{\rho c} = \frac{\rho_B c_B}{\rho c} = \frac{R_B}{\rho c} + i \frac{X_B}{\rho c} \quad (19)$$

where

$$R_B/\rho c = 1. + 0.05854(f\rho/P)^{-0.75}$$

$$X_B/\rho c = 0.08777(f\rho/P)^{-0.73}$$

and

$\rho_B c_B$ characteristic impedance in the bulk material

$f\rho/P$ dimensionless parameter

f frequency, Hz

P linear part of dc flow resistance per unit thickness of the material

The propagation coefficient in the bulk absorber is given by

$$\gamma = \alpha_B + \beta_B \quad (20)$$

where

$$\alpha_B = 0.19478k(f\rho/P)^{-0.59}$$

$$\beta_B = k[1. + 0.09476(f\rho/P)^{-0.7}]$$

These formulas are based on the results in reference 8.

Effects of Mean Flow on Impedance

For turbofan engines, where the mean flow is normally at Mach number M of 0.3 to 0.4, the resistance of nonlinear face-sheet materials on SDOF treatment panels is set by the grazing flow Mach number. The reactance is also affected by the end correction per equation (17), and the effect is large enough to shift the panel tuning frequency. The researcher is referred to references 7 and 13–19 for extensive discussion of this subject.

The practicing engineer who “needs a number” may find that the following relatively simple expressions for face-sheet resistance and for end correction to mass reactance are sufficiently accurate to be of practical use for typical designs in turbofan engines:

$$\frac{R}{\rho c} = \frac{0.3M}{\sigma} \quad (21)$$

$$\epsilon = 0.85 \frac{(1 - 0.7\sqrt{\sigma})}{1 + 305M^3} \quad (22)$$

Equations (21) and (22) are from reference 16.

Some heretofore unpublished data, summarized in table 1, support the general validity of this approach. Also, as discussed in the derivations and interpretations in the next section, these data permit a more complete description of the combined effects of flow and SPL for real treatment materials having both linear and nonlinear properties. The table includes both measured data and predictions from the relationships derived in the following section.

Combined Effects of Mean Flow and Sound Pressure Level

For both linear and nonlinear materials, it has been generally accepted that the dc flow resistance is equal to the ac resistance of the sheet in the absence of flow, a fact verified by normal-incidence impedance measurements for pure tone excitation. The dc flow resistance parameters A and B from equation (8) provide the necessary information on the relative importance of the linear and nonlinear components. We can use these facts and the definition of impedance to derive an expression relating the panel resistance to the incident SPL and grazing flow turbulence.

Starting with the definition of impedance,

$$\frac{Z}{\rho c} = \frac{p}{\rho c V_i} = \frac{R}{\rho c} + i \frac{X}{\rho c} = \theta + i\chi$$

we multiply through by V_i , take the absolute value of both sides, and solve for V_i to obtain

$$|V_i| = \frac{|p|}{\rho c \sqrt{\theta^2 + \chi^2}} \quad (23)$$

Substituting this into equation (8) gives

$$\frac{R}{\rho c} = \theta = A + \frac{Bp}{\rho c \sqrt{\theta^2 + \chi^2}} \quad (24)$$

Normal-incidence impedance measurements have shown that equation (24) correctly handles the effect of reactance on the resistance for pure tone excitation. This equation can be rearranged in the following form:

$$(\theta - A)\sqrt{\theta^2 + \chi^2} - \frac{Bp}{\rho c} = 0 \quad (25)$$

For perforate face sheets used on turbofan engine ducts, the value of A from equation (15) is negligible, and the face sheet is essentially nonlinear. The resistance is dominated by the value of B from equation (16) and the excitation pressure p . If, further, the reactance X is zero, the resistance of the perforate is a maximum, and is given at this point by

$$\theta = \frac{R}{\rho c} = \sqrt{\frac{Bp}{\rho c}} \quad (26)$$

At other frequencies, where the reactance is not zero, the resistance for pure tone excitation is smaller, as indicated by equation (24) or (25).

For wire-mesh face sheets of very fine weave, the value of B from equation (16) can ideally be made negligible, and the face sheet is essentially linear. The resistance is dominated by the value of A , that is,

$$\theta = \frac{R}{\rho c} = A \quad (27)$$

and the resistance is constant, independent of reactance, SPL, or flow effects. Purely linear materials, of course, are not available, and the discussion in reference 20 is of interest.

For real materials, whether perforate or wire mesh, neither A nor B is zero, and all real sheet materials exhibit a combination of linear and nonlinear properties so that the excitation pressure p must be taken into account. In the absence of grazing flow, the magnitude of the pressure (in dynes/cm²) can be obtained from the SPL of the incident wave as

$$|p| = (2 \times 10^{-4})10^{(\text{SPL}/20)} \quad (28)$$

The agreement between the measured resistance values in table 1 and predictions by equations (24) and (28) is shown in figure 6. These data, for pure tone excitation, show the nonlinear effect of sound pressure level and the variation of resistance with frequency stemming from the effect of the reactance term χ in equation (24). Further

Table 1. Combined Flow and SPL Effects on Predicted and Measured Impedance for a 6.7-Percent Perforate

[Data obtained with apparatus in fig. 12
 Cavity depth = 1.0 in.; Hole diameter = 0.032 in.
 Face-sheet thickness = 0.032 in.; Porosity = 6.7%
 A = 1.4; B = 0.2336]

Frequency, Hz	$M = 0$					$M = 0.2$				
	OASPL	$R/\rho c$		$X/\rho c$		OASPL	$R/\rho c$		$X/\rho c$	
		Meas.	Pred.	Meas.	Pred.		Meas.	Pred.	Meas.	Pred.
1100	146.9	0.37	0.39	-1.5	-1.50	146.7	0.77	0.49	-1.45	-1.51
	142.2	.24	.24	-1.49	-1.50	141.7	.69	.39	-1.45	-1.50
	137.0	.17	.13	-1.46	-1.49	136.1	.66	.34	-1.44	-1.50
	126.8	.13	.04	-1.43	-1.47					
1350	151.5	.71	.79	-1.05	-1.05	146.7	.77	.64	-1.02	-1.04
	146.5	.47	.51	-1.03	-1.04	141.2	.70	.52	-1.01	-1.04
	141.6	.31	.31	-1.02	-1.03	135.9	.65	.46	-1.00	-1.03
	136.4	.21	.18	-.98	-1.02					
	126.4	.14	.06	-.94	-.99					
1750	141.6	.44	.48	-.45	-.49	147.1	.92	.83	-.5	-.51
	136.7	.31	.33	-.48	-.47	141.7	.81	.70	-.48	-.50
	126.4	.19	.12	-.43	-.45	135.8	.75	.65	-.47	-.50
2100	139.9	.48	.52	-.13	-.12	140.8	.78	.76	-.16	-.14
	136.5	.40	.42	-.12	-.11	136.2	.74	.72	-.12	-.14
	126.7	.25	.24	-.07	-.08					
2450	141.6	.52	.56	.11	.18	141.7	.71	.77	.12	.16
	136.5	.39	.41	.14	.20	136.1	.62	.72	.11	.17
	126.7	.25	.19	.21	.24					
2700	139.6	.32	.45	.39	.39	139.7	.67	.71	.3	.36
	126.8	.21	.13	.44	.44	136.0	.64	.68	.3	.37
3000	136.7	.30	.27	.66	.63	137.8	.61	.63	.46	.59
	126.7	.20	.09	.71	.68	135.9	.59	.62	.45	.59
3200	140.3	.17	.34	.83	.76	136.1	.53	.57	.67	.74
	131.5	.10	.13	.85	.81					

Table 1. Concluded

Data obtained with apparatus in fig. 12
 Cavity depth = 1.0 in.; Hole diameter = 0.032 in.
 Face-sheet thickness = 0.032 in.; Porosity = 6.7%
 $A = 1.4$; $B = 0.2336$

Frequency, Hz	$M = 0.3$					$M = 0.4$				
	OASPL	$R/\rho c$		$X/\rho c$		OASPL	$R/\rho c$		$X/\rho c$	
		Meas.	Pred.	Meas.	Pred.		Meas.	Pred.	Meas.	Pred.
1100	145.4	0.92	0.73	-1.13	-1.51	146.3	0.93	1.10	-0.98	-1.52
	141.5	.86	.70	-1.14	-1.51	142.1	.68	1.08	-.98	-1.52
1350	146.9	1.04	.92	-.76	-1.05					
	141.8	.94	.86	-.72	-1.05					
1750	140.9	1.11	1.02	-.27	-.52	144.2	.95	1.38	-.13	-.53
						141.3	.86	1.37	-.13	-.53
2100	141.4	1.11	1.07	0	-.16	143.7	1.28	1.42	.33	-.18
2450	146.3	1.08	1.12	.23	.14	150.2	1.43	1.48	.37	.12
	141.4	1.02	1.08	.23	.14					
2700	140.3	.97	1.05	.33	.34	143.1	1.31	1.41	.61	.32
3000	140.1	1.01	1.00	.50	.56	142.8	1.34	1.37	.77	.54
3200						142.6	1.31	1.35	1.01	.68

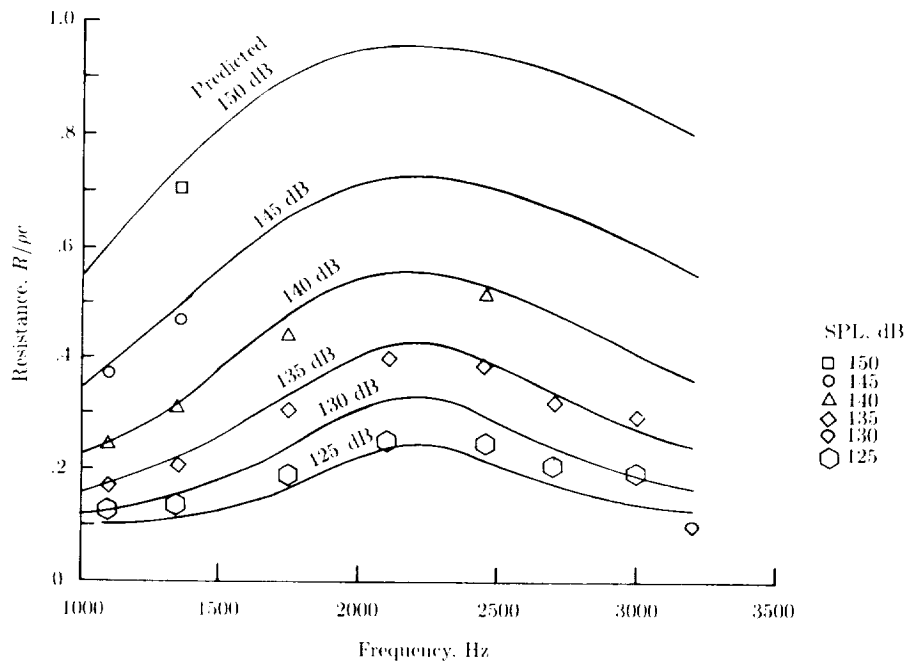


Figure 6. Effects of SPL on resistance of SDOF panel with nonlinear face sheet. Perforate properties: $A = 1.4$, $B = 0.2336$, $t = 0.032$ in., $d = 0.032$ in., $\sigma = 6.7$

research is needed to determine whether the effect of reactance on resistance is still present for broadband excitation.

The data in table 1 at zero flow show a systematic effect of SPL on the reactance. These data, augmented by similar data at two additional porosities, are shown in figure 7 in terms of the effect of incident velocity V_i on the end correction ϵ . Note that the data correlation indicates that the prior correlation by Ingard (eq. (18)), using porosity as a parameter, could be replaced by a relationship involving the face-sheet resistance as it affects the velocity incident on the panel; that is,

$$\epsilon = \begin{cases} 0.85 & (V_i < 0.4 \text{ cm/sec}) \\ 0.738 - 0.119 \ln V_i & (0.4 \text{ cm/sec} \leq V_i \leq 493 \text{ cm/sec}) \\ 0 & (V_i > 493 \text{ cm/sec}) \end{cases} \quad (29)$$

The value of V_i is determined by

$$V_i = \frac{p}{\rho c \sqrt{\theta^2 + \chi^2}} \quad (30)$$

The flow turbulence associated with the grazing flow results in a pressure excitation that causes the resistance to increase just as if SPL were increased. As shown by Rice, the effect of flow Mach number M is as given by equation (21).

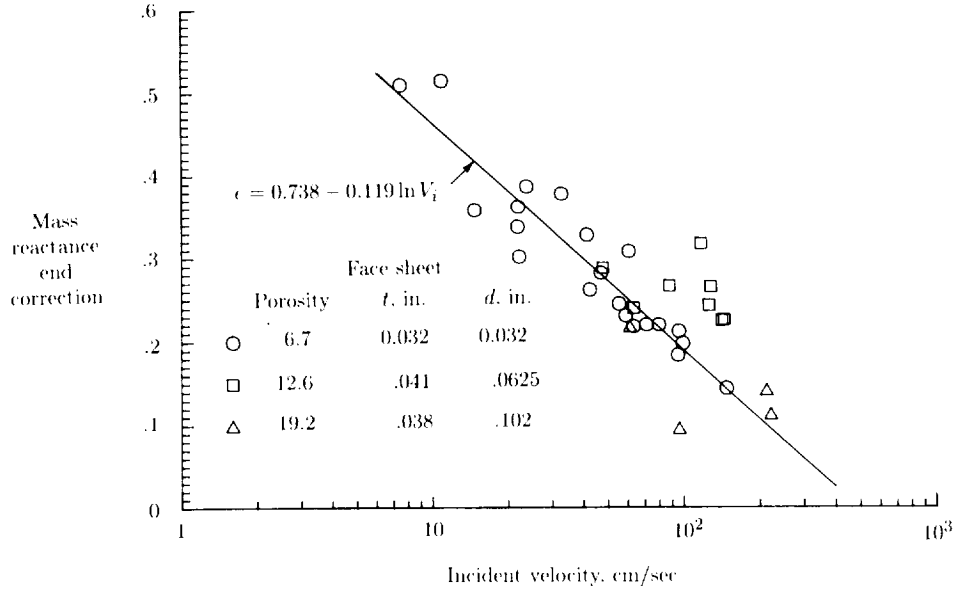


Figure 7. Effect of incident velocity on mass reactance end correction.

To further establish the effects of flow and SPL, data were obtained using the in situ impedance measurement system to be described subsequently. The experimental data for a 6.7-percent-porosity face sheet are summarized in table 1 together with results of prediction by a method to be described in the following paragraphs.

The effect of flow turbulence on the total excitation pressure p_T is assumed to add on an energy basis with that from simple acoustic excitation; that is,

$$p_T = \sqrt{p_A^2 + p_F^2} \tag{31}$$

where

p_A acoustic pressure from equation (28)

p_F flow turbulence pressure fluctuation

This is similar to the root-mean-squared velocity considered in reference 17.

The experimental data in table 1, for flow Mach numbers of 0, 0.2, 0.3, and 0.4, were used to estimate the magnitude of the turbulence effect. It was determined that a good fit was obtained between predicted and measured resistance as a function of Mach number, including the effect of SPL from equation (31), when the value of p_F was

$$p_F = 90\,000 M^2 \tag{32}$$

As pointed out in reference 17, the value of the constant should take into account the boundary layer profile, and further research is required to improve equation (32). Nevertheless, the agreement between predicted and measured data can be seen,

in total, in table 1; the measured data show a strong increase in resistance with increasing Mach number that is reasonably well predicted, even at Mach 0.4. The additional effect of SPL as predicted by equation (31) is also demonstrated.

A more graphic demonstration of the relatively good agreement is given in figure 8 for Mach 0.3. Note that in both table 1 and figure 8 the predicted variation of resistance with frequency, and hence reactance, is reasonably well confirmed.

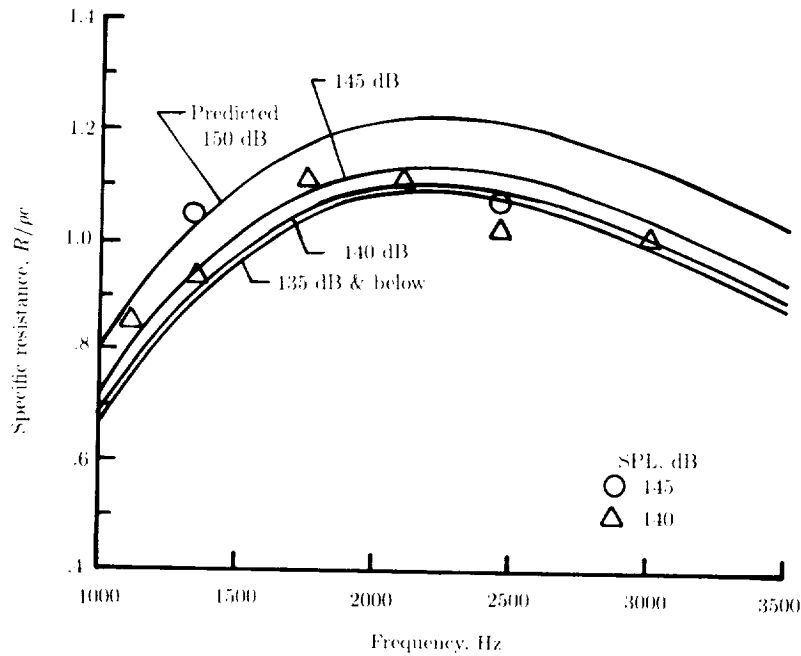


Figure 8. Predicted and measured resistance of a perforate versus frequency at Mach 0.3.

It should be noted that equation (26) can be put into the same form as equation (21) for a simple perforate using equations (16) and (32) (for the case of zero reactance) as follows:

$$\frac{R}{\rho c} = \sqrt{B \frac{p}{\rho c}} = \sqrt{\frac{(K_i + K_e) 90\,000}{2cC_D^2 \rho c} \frac{M}{\sigma}} \quad (33)$$

When we set $K_i + K_e = 1$, $\rho c = 41.5$ rayls, $c = 34\,380$ cm/sec, and $C_D = 0.76$, the constant factor becomes 0.24, which is within 80 percent of Rice's value of 0.3 in equation (21).

The predicted reactances in table 1 used equations (29) and (30) to determine the mass reactance end correction and used equation (31) to determine the pressure. The prediction results in a decrease in reactance with increasing Mach number; the data suggest a small increase. Further research on this aspect of flow effects is needed.

Another feature of perforate face sheets illustrated by equation (26) is that the square root permits both a positive and a negative answer:

$$\frac{R}{\rho c} = \pm \sqrt{\frac{pB}{\rho c}} \quad (34)$$

The existence of a negative square root solution implies a negative resistance, suggesting noise generation rather than absorption. For linear materials, with a significant value of A , noise generation is not a problem. Under the right conditions, noise generation has been observed experimentally many times and generally consists of a tone whose frequency is given by a dimensionless Strouhal number N_{St}

$$N_{St} = \frac{fd}{V_{\infty}} \quad (35)$$

where V_{∞} is the mean flow velocity. In reference 18, N_{St} was found to be approximately 0.2. In reference 19, the tone occurred at the resonant frequency (i.e., $X = 0$) for $N_{St} = 0.26$. Extensive experimental studies of the occurrence of this phenomenon have also been reported in reference 21.

Measurement of Liner Impedance

The impedance of acoustic treatment panels can be determined experimentally in several ways: (1) by measurement of the dc flow resistance of the constituents of the panel for input to an analytical impedance model (as discussed in the preceding section), (2) by measurement of the standing wave pattern in a normal-incidence impedance tube using either a traversing probe or two (or more) fixed pressure transducers, and (3) by measuring the in situ impedance with sensors attached to the face sheet and inside the panel cavity. The first two methods are suitable when grazing airflow effects on the face sheet are of negligible concern; the last method permits impedance measurement in a duct, either in the laboratory or in the engine.

Direct Current Flow Resistance Measurement

A typical test apparatus for dc flow resistance measurement is shown in figure 9 (ref. 22). The sample panel is placed in a sample holder, which has a well-defined cross-sectional area. Then air is driven through the sample either by a pressurized line or a vacuum line, as shown, and metered by the flowmeter. The pressure drop across the sample is determined by a differential pressure measuring device. The dc flow resistance is then determined by

$$R = \frac{\Delta p}{V_i} \quad (36)$$

where Δp is the pressure drop across sample in dynes/cm². It is assumed that V_i has been correctly determined by accounting for the volume flow as measured in the flowmeter and the cross-sectional area of the sample.

As pointed out in reference 10, plotting R versus V_i results in a linear function of the form given in equation (8). The coefficients A and B can be determined by

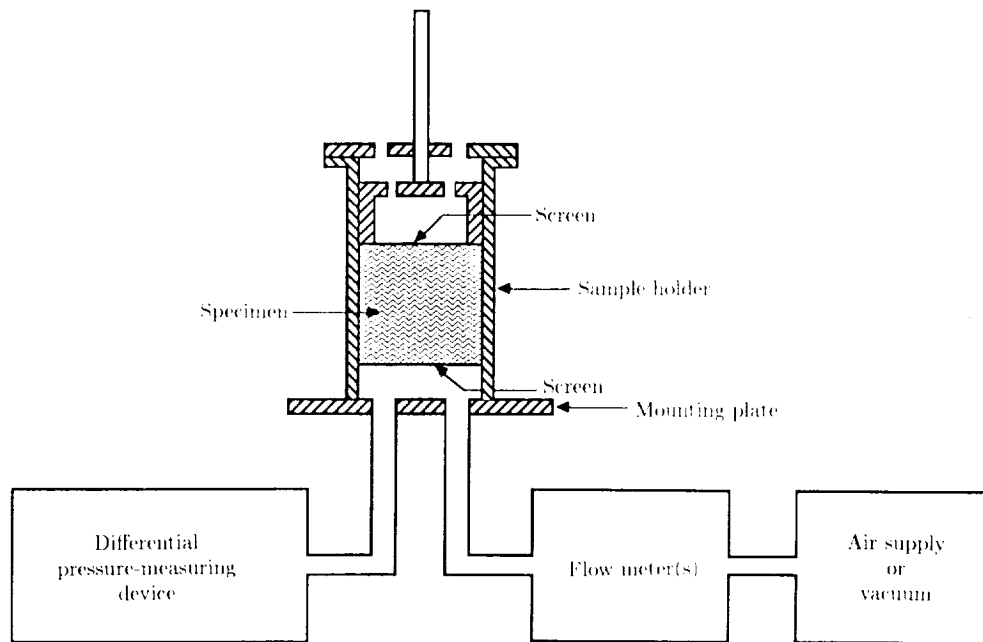


Figure 9. Apparatus for measuring flow resistance. (From ref. 22. Copyright ASTM. Reprinted with permission.)

a linear curve fit to the measured data. When the porosity of the sample is smaller than 5 to 10 percent, compressibility effects can cause an apparent departure from this simple relationship; a method for eliminating this difficulty in the measurement is described in reference 11.

Normal-Incidence Impedance Measurement

Single-sensor method: The apparatus shown in figure 10 (ref. 7) is representative of systems used for determination of impedance by reflection of normal-incidence sound waves. Sound introduced at the source end of the tube travels in a plane wave and reflects from the end containing the test sample, setting up a standing wave pattern along the length of the tube that depends on the strength and phase of the reflected wave. The traversing probe is used to measure the maximum and minimum sound pressure levels of the standing wave pattern and the distances from the face sheet of the sample to the location of the minima.

The pressure of the standing wave pattern in the tube is described by (ref. 4)

$$p(x) = \left[(A + B)^2 \cos^2 \left(kx + \frac{\phi_{BA}}{2} \right) + (A - B)^2 \sin^2 \left(kx + \frac{\phi_{BA}}{2} \right) \right]^{1/2} \quad (37)$$

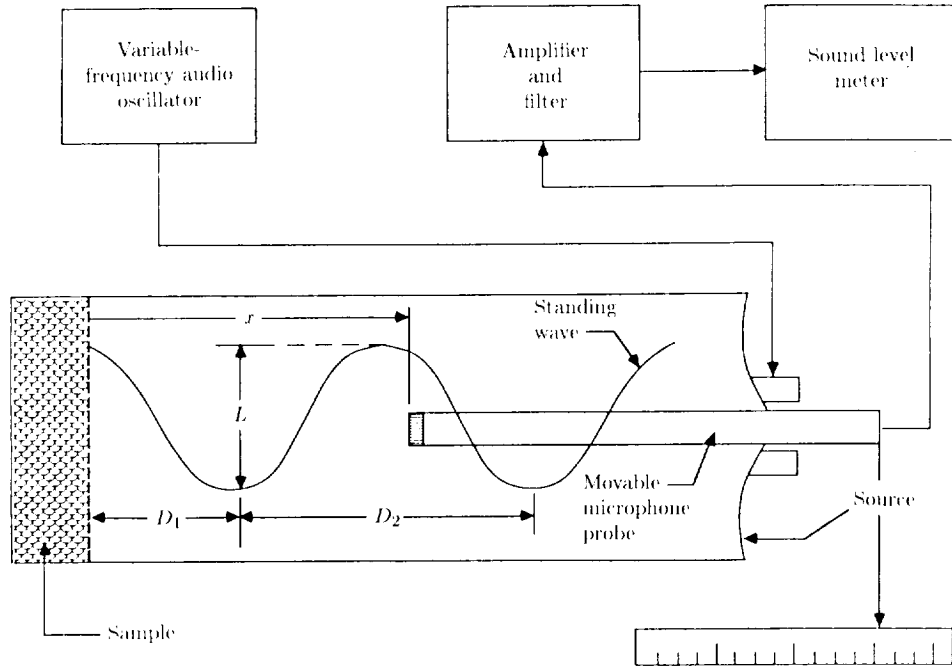


Figure 10. Normal-incidence impedance tube apparatus. (From ref. 7.)

where

- p standing wave pressure amplitude, dynes/cm²
- A amplitude of incident wave, dynes/cm²
- B amplitude of reflected wave, dynes/cm²
- x distance from surface of test sample, cm
- ϕ_{BA} phase angle between incident and reflected pressure waves, radians

The impedance is given by

$$\frac{Z}{\rho c} = \frac{A + Be^{i\phi_{BA}}}{A - Be^{i\phi_{BA}}} \quad (38)$$

The magnitude of B relative to A is determined from the measured standing wave ratio (SWR):

$$\text{SWR} = \frac{A + B}{A - B} \quad (39)$$

where $A + B$ is the maximum of the standing wave pattern and $A - B$ is the minimum of the standing wave pattern. Rearranging equation (39), we get

$$\frac{B}{A} = \frac{\text{SWR} - 1}{\text{SWR} + 1} \quad (40)$$

(The standing wave ratio is usually measured as the number of decibels between the peak and the null and must be converted to a ratio in pressure units for use in eq. (40).)

The phase of the reflected wave relative to the incident wave, ϕ_{BA} , is determined from the position of the first minimum, $x = D_1$ (shown in fig. 10). This first node occurs where, in equation (37)

$$kD_1 + \phi_{BA}/2 = -\pi/2$$

so that

$$\phi_{BA} = -(\pi + 2kD_1) \quad (41)$$

is the phase angle that the reflected wave leads or lags the incident wave. The results in equations (40) and (41) provide the information needed in equation (38) to determine the impedance.

Because this method depends on examining a standing wave pattern, it is limited to discrete frequencies; for that reason, in design work it has generally been discarded in favor of the dual-sensor method, described next. The data analysis and the correction for sound absorption in the tube are further discussed in references 23 and 24.

Dual-sensor method: A test setup for the dual-sensor impedance tube method is diagrammed in figure 11. A random noise signal is input from one or two speaker sources as shown in the top half of the figure. A digital thermometer is included because of the need to determine the speed of sound accurately. The bottom half of the figure shows the measurement system, which includes a fixed pressure sensor mounted flush on the wall and a translating probe-mounted sensor. The two signals are amplified and processed in a two-channel spectral analyzer that permits determination of the impedance over the full range of frequencies of interest with a single measurement. The method is discussed further in references 25, 26, and 27.

The value of impedance at a given frequency depends on the pressures at the two sensors, the phase between the two, and their separation distance and is given by

$$\frac{Z}{\rho c} = \frac{i \left[\sin(kx_1) - \frac{p_1 p_2 e^{i\phi_{12}}}{p_2^2} \sin(kx_2) \right]}{\frac{p_1 p_2 e^{i\phi_{12}}}{p_2^2} \cos(kx_2) - \cos(kx_1)} \quad (42)$$

where

x_1, x_2 distance from sample face of sensors 1 and 2, cm

p_1, p_2 pressure amplitude at sensors 1 and 2, dynes/cm²

ϕ_{12} phase angle between pressure sensors 1 and 2, radians

The quantity $p_1 p_2 e^{i\phi_{12}}$ is the cross spectral density of the two pressure signals and p_2^2 is the auto spectral density of p_2 . Many types of two-channel analyzers are available

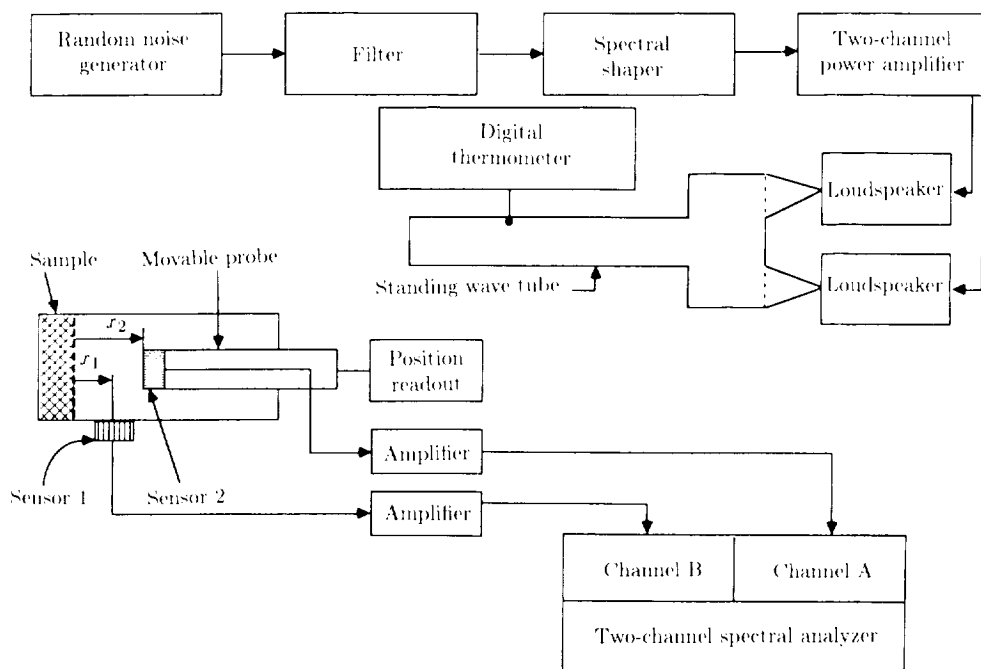


Figure 11. Dual-sensor method for normal-incidence impedance measurement.

to provide the information in equation (42), and the measurement can easily be automated using a microcomputer-based system.

Locating sensor 1 as close as practicable to the face sheet of the treatment sample gives an indication of the SPL exciting the panel and allows investigations of panel nonlinearity. Note that the measurement ideally requires only two sensors at the fixed positions x_1 and x_2 . The recommendation that sensor 2 be on a movable probe, permitting variation of x_2 , arises from the fact that at certain combinations of sample impedance and frequency, x_2 may fall at a null of the standing wave pattern, giving potential signal-to-noise-ratio sensitivity problems. Being able to vary x_2 avoids this problem and permits a means to verify measurement repeatability, since the results should be independent of x_2 .

An inherent limitation of both single- and dual-sensor impedance tube methods is the upper frequency limit of the measurement. The measurement requires the presence of plane-wave propagation in the tube, so that the upper frequency limit is a conservative factor (roughly 0.75) times the frequency at which the first higher order mode begins to propagate. In a standard 1.0-inch-diameter tube at room temperature, the first mode above the plane wave (lowest radial mode of the first order circumferential mode) cuts on at about 8000 Hz, limiting the useful upper frequency to about 6000 Hz. The upper frequency limit can be increased by using a smaller diameter tube, but care must be taken that the treatment sample is not too small to be representative of an average panel area.

In Situ Impedance Measurement Systems

The apparatus shown in figure 12 is representative of that used for determination of impedance by the more specialized in situ method often called the two-microphone method. This method is most often used when information is required about the effects of grazing flow on the treatment impedance and can be used in a laboratory duct or on the actual engine installation. It is similar to the dual-sensor method discussed in the preceding section, but in this case both sensors are fixed within the panel itself. One sensor is mounted flush on the backplate of a chosen cavity (microphone B) and the other is inserted through the face sheet (microphone A). The sensors must be small enough to have negligible effects on the propagation within the cavity.

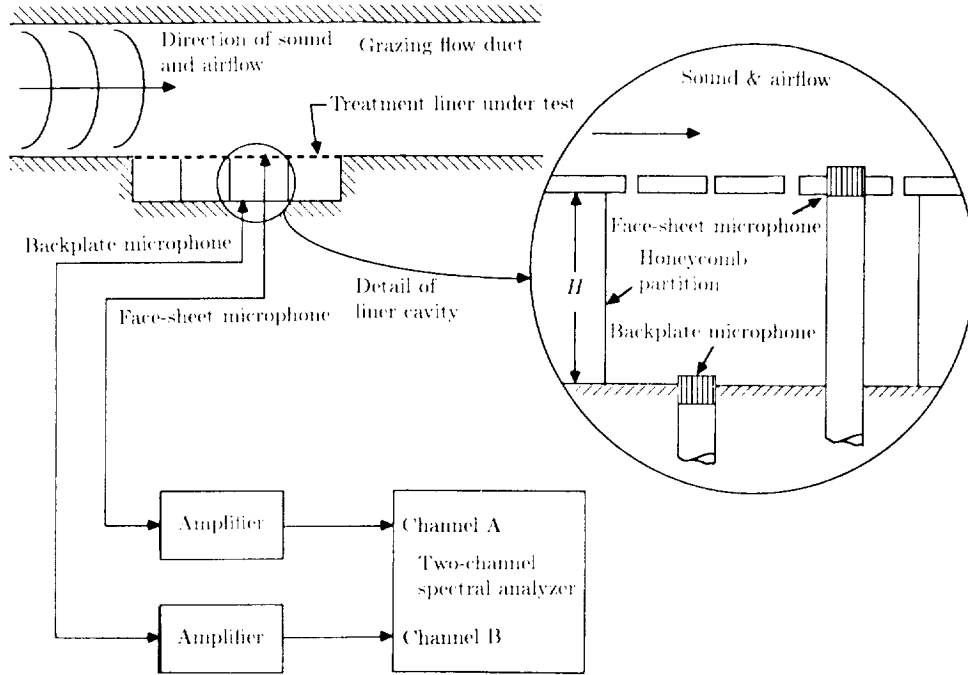


Figure 12. Measurement of grazing flow impedance by two-microphone method.

A two-channel spectral analyzer is used to obtain the amplitude and phase of the two pressure signals relative to one another. In this case the impedance for an SDOF panel is related to the measured quantities by the expression

$$\frac{Z}{\rho c} = -i \frac{p_A p_B e^{i\phi_{AB}}}{p_A^2 \sin(kh)} \quad (43)$$

where $p_A p_B e^{i\phi_{AB}}$ is the cross spectral density between microphones A and B, p_A^2 is the auto spectral density of microphone A, and h is the panel depth. Further

discussion of the method and the extension of the method to 2DOF linings is given in references 13, 14, and 28.

Empirical and Semiempirical Design Methods

Development of Design Data Bases and Charts

In the earlier section on empirical and semiempirical design approaches, the manner of evolving designs from experimental data bases was discussed. The scope of the general design problem includes the fan or compressor inlet, the fan exhaust, and the core engine exhaust. Experimental facilities for conducting these tests are discussed subsequently.

The inlet and fan exhausts are at temperatures and pressures reasonably close to ambient laboratory conditions, so that only relatively small errors are introduced if laboratory data are not corrected. In contrast, the core exhaust is always at such high temperature and, usually, elevated pressure that either tests must be conducted under the engine conditions or appropriate analytical corrections must be made to (1) the properties of the treatment and (2) the duct propagation effects.

The scaling parameter for conducting experiments at ambient or elevated conditions is the ratio of duct diameter or duct height to wavelength (D/λ or H/λ). The wavelength at a given frequency depends on the temperature in the duct.

With this in mind, contours of isosuppression can be determined to establish design data bases or design charts as described previously. An example of such a contour plot is given in figure 13, showing isosuppression contours in the impedance plane (reactance versus resistance) at a 1/3-octave band frequency of 4000 Hz and for mean flow of Mach 0.3. To generate the plot, treatment cavity depths of 0.25 inch through 1.0 inch were tested, in each case with seven wire-mesh face-sheet resistances. These variations provided data for magnitude of suppression at the intersections of the grid that were used to draw the isosuppression contours. Similar plots can be created for a range of 1/3-octave band frequencies and airflow Mach numbers. In this form, the data allow peak suppression and associated optimum resistance and reactance to be empirically determined as a function of frequency and can be used to obtain the suppression sensitivity to nonoptimum impedance.

These data can be normalized with dimensionless parameters as illustrated in figure 14, showing the ratio of peak suppression in decibels to the ratio of duct length to height as a function of duct height-to-wavelength ratio (H/λ). Figure 15 shows the optimum resistance ($R/\rho c$) versus H/λ . A similar plot can be constructed for the optimum reactance. In practice, curve fits are made for computerization of such data including the nonoptimum contours, so that by predicting the impedance candidate treatment panel designs, the associated suppression spectrum can be quickly estimated.

Reference 29 presents an excellent summary of methods developed by Rice and others to enable analytical estimation of the peak suppression, optimum impedance, and bandwidths of suppression for particular treatment designs. These methods, when applied to inlets, lead to a "cutoff-ratio" correlating parameter that has been

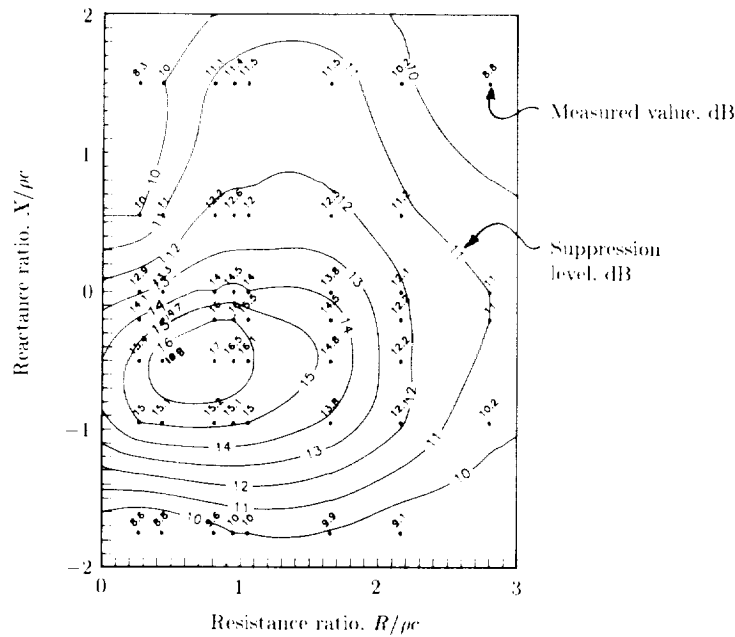


Figure 13. Example of isosuppression contours drawn in impedance plane.

recognized to be closely related to wave angles associated with the ray acoustics approach.

Reference 29 is recommended to the designer interested in closed-form solutions for suppression representing curve fits to extensive parametric study results. These studies are based on modal analysis and are correlated in terms of cutoff ratio, duct Mach number, and treatment impedance. Rice has also evaluated the effects of boundary layer thickness.

In reference 30, the ray acoustics approach was pursued for turbofan two-dimensional ducts. Such methods are in the semiempirical category, requiring an assumption about the modal energy distribution. The advantage of this approach is the reasonably good results obtained for engines, as well as the rapid computer predictions that result from this simplified calculation procedure.

Design Procedures

Choice of Suppressor Design Frequencies

Even after features have been incorporated to reduce noise at the source, turbofan engines have strong tonal content in the noise spectrum. These tones occur at the blade-passage-frequency (BPF) harmonics of the turbomachinery rotating blades. Problem sources are the fan itself, the booster stages feeding air into compressor, sometimes the front stages of the compressor, and the turbine stages. When there is more than one stage in series, nonlinear effects introduce sum and difference frequencies of the tone harmonics from the individual stages.

The usual design problem, fortunately, is limited to the fan stage fundamental BPF and one or two higher harmonics. If noise at only the BPF and next

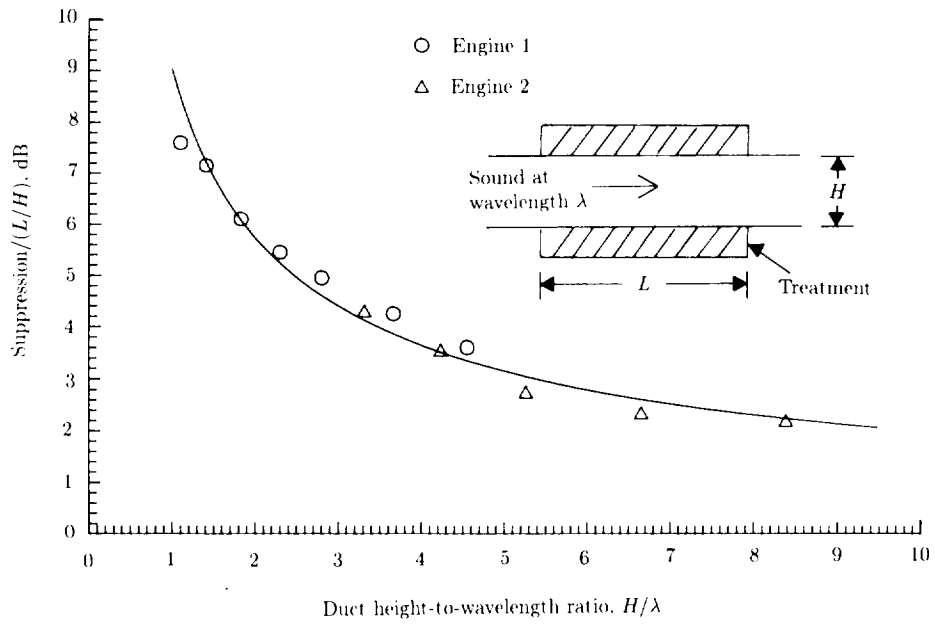


Figure 14. Ratio of maximum measured suppression to ratio of duct length to height for optimum impedance versus H/λ in fan exhaust ducts.

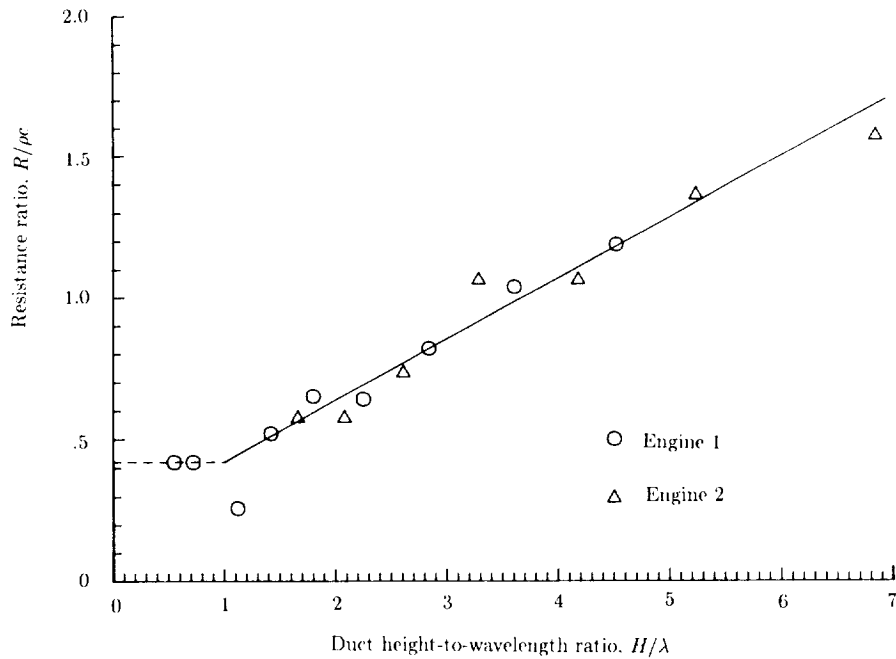


Figure 15. Optimum resistance versus H/λ as measured in fan exhaust duct.

10 K.

mm
 130
 a
 /

harmonic must be reduced, the single-layer SDOF panel construction is chosen. If noise at the BPF and both higher harmonics must be reduced, the dual-layer 2DOF panel construction is chosen. Broadband noise from turbomachinery is almost exclusively associated with the sideband frequencies on either side of the tone harmonics, and a design aimed at the tones is also effective for the broadband component.

Determination of Liner Design Parameters

The process to be used for selecting design values for the duct treatment acoustic impedance, both resistance and reactance, has been briefly discussed. These discussions are based on the concept of selecting the impedance parameters to achieve the largest reduction of sound within the duct itself. Actually, for turbofan engine noise, the effect of far-field directivity must also be taken into account.

When the propagating energy is comprised primarily of broadband noise in uncorrelated propagating modes (e.g., involving phase modulation by turbulent mixing layers or by unsteady inlet conditions), the angle of far-field radiation for each mode and the relative energy distribution among those modes become a primary concern. The emphasis on which modes to suppress depends on whether the inlet or the exhaust is being considered.

In the inlet, where the sound wave is propagating against the flow, the flow boundary layer tends to refract the waves toward the axis of the duct, decreasing their propagation angle and effectively converting them into lower order radial modes. In the exhaust duct, where the sound propagates with the flow, the boundary layer tends to refract waves toward the wall, increasing their propagation angle and effectively converting them into higher order modes. These phenomena affect the design philosophies for inlet and exhaust differently.

Inlet suppression: Modes that radiate from the inlet to the far field aft of about 50° from the inlet axis require more suppression than those radiating forward of that angle, because modes at higher propagation angles reach locations on the ground that receive the loudest noise levels during aircraft takeoff. Fortunately, the higher order modes, which are easier to suppress, have higher propagation angles in the duct and thus require more suppression than the lower order modes. Lower order modes and those modes refracted toward the inlet axis are less of a problem because of the long propagation distance to the ground associated with shallow radiation angles.

In reference 30, the correspondence is shown between the modal theory and the ray acoustics solution, as illustrated in figure 16. The figure shows the mean-square pressure measured on a far-field arc as a function of angle from the duct centerline. When these levels are transformed to a sideline plot (more representative of an aircraft flyover), the peak levels from the treated duct occur at 40° to 50°. As first approximation, these angles correspond to the same angles within the duct from simple acoustics and based on equation (3), the resistance to obtain optimum suppression at these angles should be

$$1.30 = (\sin 50^\circ)^{-1} \leq R_{opt}/\rho c \leq (\sin 40^\circ)^{-1} = 1.56$$

The optimum reactance should be near zero or slightly negative at the frequencies of concern.

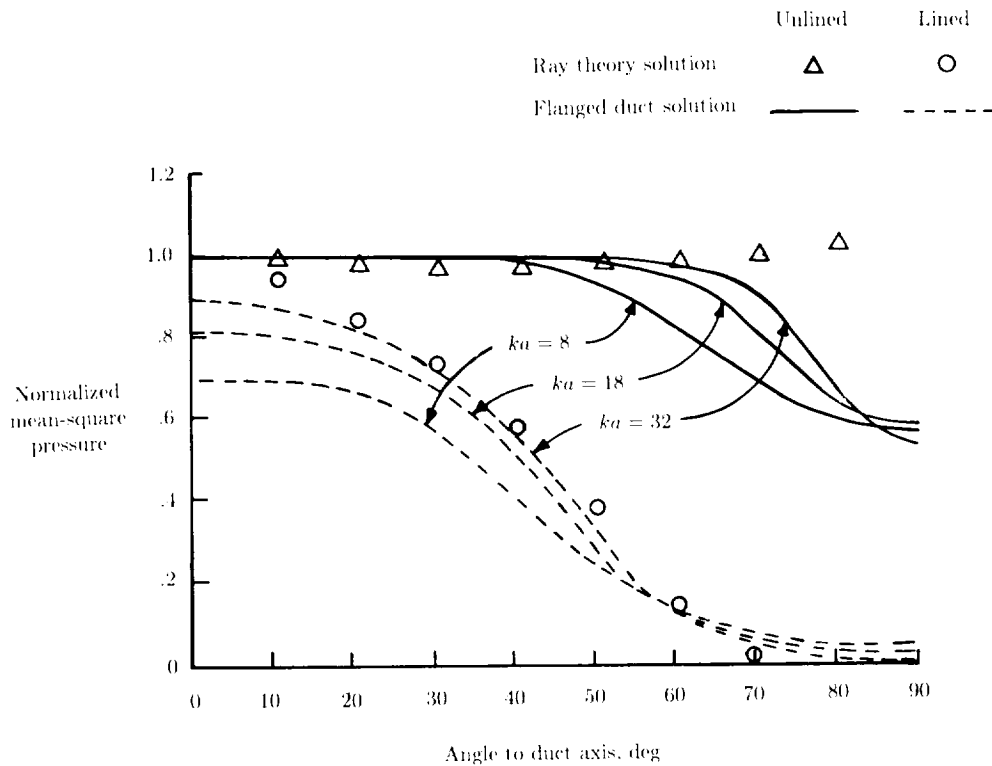


Figure 16. Comparison of ray theory and “flanged-duct” solutions for monopole sources in a cylindrical duct for various values of wave number times radius, ka . $L/a = 1$; $Z/\rho c = 0.8 + 0.4i$; mean-square pressure normalized for radius = $\lambda/4\pi\phi$. (From ref. 30. Copyright AIAA. Reprinted with permission.)

Exhaust suppression: In the exhaust, the higher order modes are refracted by the boundary layer to even higher propagation angles, increasing their attenuation rates. Therefore, the lower order modes present the greater problem, and rigorous analysis must consider modal propagation in nonuniform ducts with nonuniform flow and thus requires extensive computational capability.

The engineering solution is obtained by maximizing the suppression of noise within the duct, usually by testing a mock-up duct. This generally results in optimum suppression for the far-field radiated noise as well, excepting only very unusual problems with source mechanisms that happen to generate particularly high-amplitude higher order modes.

Total inlet or exhaust suppression: The treatment lengths needed to obtain the desired suppression are a consequence of the suppression rates achieved at the impedance values selected by the above process. To complicate this matter further, the overall suppression rates are not necessarily linear with treatment length, particularly for short treatment sections. Suppression rates may be quite high near

the beginning of a panel, as higher order modes rapidly attenuate, but gradually decrease as fewer modes contribute to the total energy. Thus, doubling the length of a short panel may not double its effectiveness.

Using Segmented Treatment Design

When two or more frequencies are so widely separated that they cannot be suppressed with either SDOF or 2DOF and when bulk absorber is not practical, use of segmented treatment in tandem is a practical approach. This might be the case in a turbine exhaust requiring suppression of both turbine tones and combustor broadband noise. Each segment of treatment must have sufficient length to achieve suppression at its design frequency. The primary deterrent to the use of segmented treatment is the normal limitation on overall duct length resulting from weight constraints.

Testing for Treatment Design and Performance Measurement

Experience has shown that treatment for fan and turbine exhaust ducts can be successfully developed by testing in the acoustic laboratory. Parametric experimental data can be obtained at a very small fraction of the cost associated with tests on an actual engine, and the results have been found to be reliable when applied to the engine, particularly if a representative sector of the exhaust duct geometry is faithfully simulated in the laboratory facility. In contrast, the inlet can be represented well enough only by testing either a scale model fan simulation or a full-scale engine.

Laboratory Testing of Exhaust Ducts

A typical test facility for the exhaust mode is shown in figure 17. The treatment is applied on the top and bottom of a small rectangular duct section, while the sides of the duct are left rigid, to simulate a circumferential segment of the exhaust annulus. The test section connects two large hard-walled plenums in which the sound levels are measured to determine the suppression provided by the treatment. Airflow is passed through the treated section to simulate engine conditions. The reverberant chambers provide a diffuse sound field, and a single microphone in each chamber is adequate for acoustic measurement; traversing the microphone assures that the data are not biased by a standing wave pattern. Suppression of a treatment design is measured by first measuring levels in the chambers with a hard-walled test section and then measuring the levels with the treatment in place. The difference in levels measured in the downstream chamber is the insertion loss of the treatment, giving rise to the term "insertion loss measurement method."

If the duct on the engine has significant curvature, disruptions of treatment, or change in duct height, higher order modes are continually regenerated. In this case, the facility test section should closely represent the duct curvature and any axial variation in duct height associated with it. Many commercial turbofan engine exhaust ducts fall into this category.

An alternative to the dual reverberation chamber method is to measure the sound pressure levels in the duct with traversing probes upstream and downstream of the

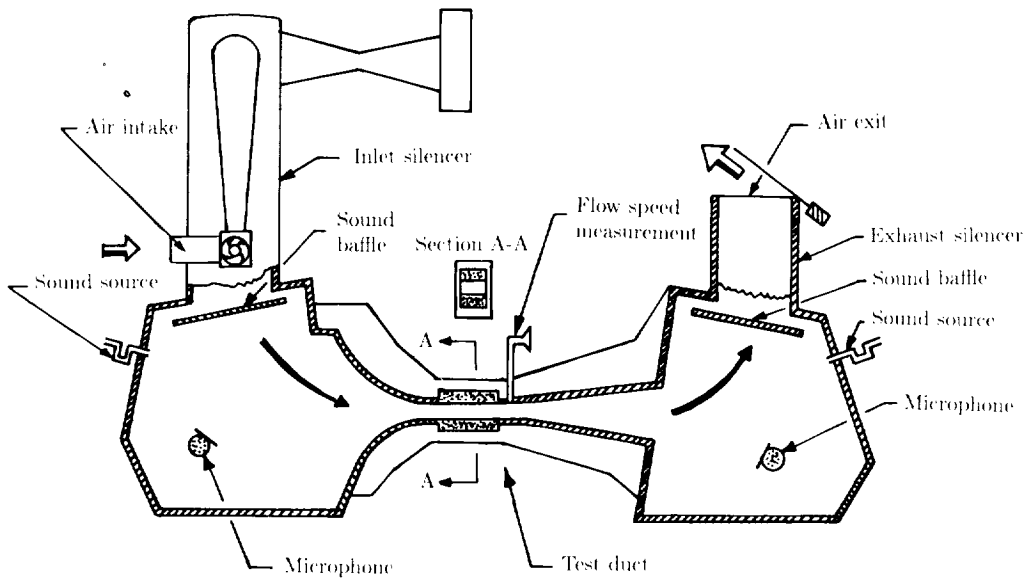


Figure 17. Typical test facility for development of exhaust duct treatment designs.

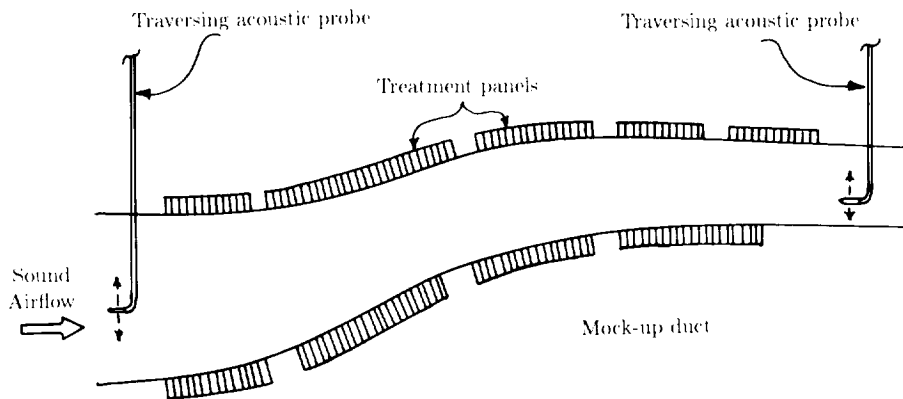


Figure 18. Typical test facility for development of treatment designs. Mock-up of curved exhaust duct.

treated section. The SPL measurement is integrated across the duct to provide estimates of the total power flux upstream and downstream of the treatment. This method is usually called the transmission loss method, as opposed to the insertion loss method described previously.

In the transmission loss method, it is assumed that backward-traveling waves have negligible effect on the measured SPL profile. Often, the transmission loss is measured in a hard-walled version of the duct at the desired flow velocity, and the transmission loss of the treated version is "corrected" by the hard-walled duct transmission loss. An example of a mock-up of such a duct is shown in figure 18.

Scale Model Test Facilities

For the inlet testing, the typical facility consists of a fan, usually a scale model, that can be motor driven, with the inlet noise radiating into an anechoic chamber. Far-field testing is essential for empirical development of inlet treatment because the wavelengths of the fan tones are small relative to the inlet diameter, and higher order modes dominate the propagating energy in the duct. In this case, actual inlet hardware, including the turbofan rotor and stator, must be closely simulated. An illustration of such a test facility is shown in figure 19. Far-field microphones are spaced along an arc to provide the essential information on the effect of the treatment on directivity.

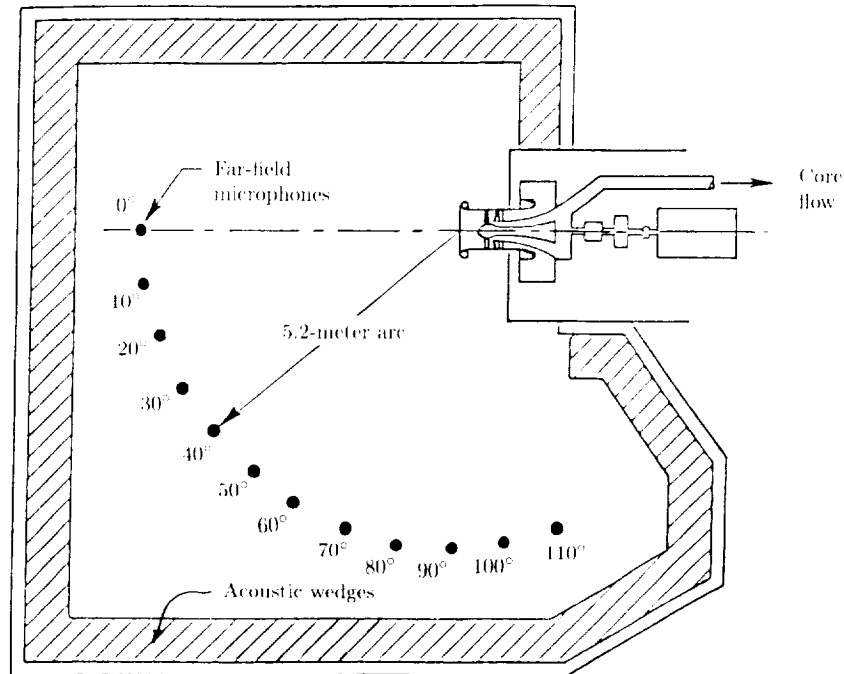


Figure 19. Typical scale model mounted in anechoic facility for development of treatment designs for inlet duct configuration.

When testing in a scale model facility in the exhaust mode, the fan inlet must have a suitably designed plenum to provide a smooth, distortion-free velocity profile into the fan, and the exhaust flow must be allowed to exit from the chamber in a way that provides good anechoic acoustics. Such an arrangement as tested in the NASA Quiet Clean Short-Haul Experimental Engine Program (ref. 31) is illustrated in figure 20.

Full-Scale Engine Tests

Full-scale engine tests for acoustic measurements are made in facilities such as in figure 21. The engine is mounted on a static test stand at the center of a far-field

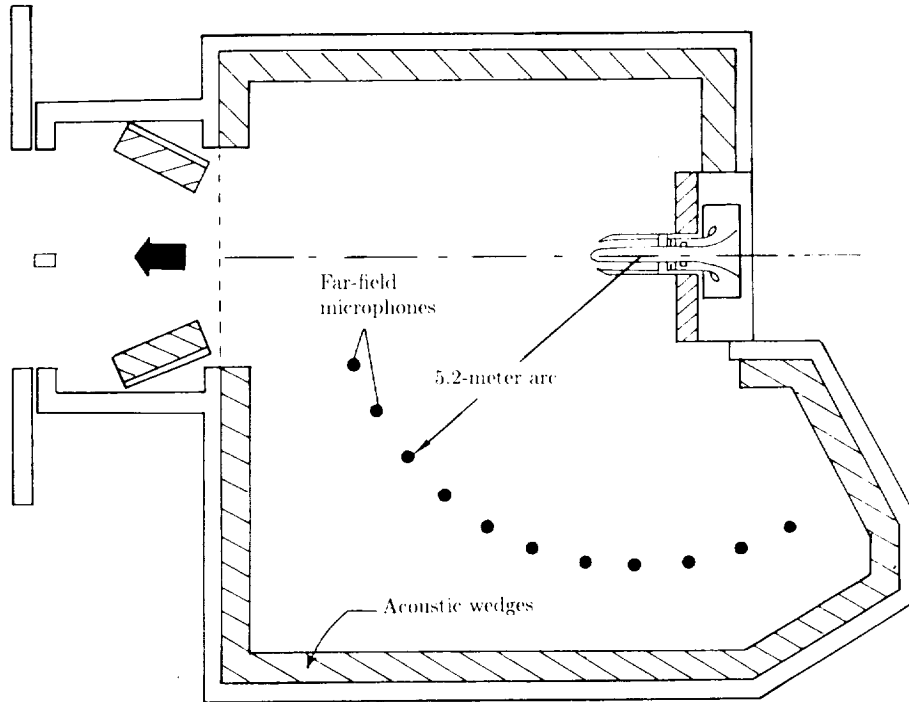


Figure 20. Typical scale model mounted in anechoic facility for development of treatment designs for exhaust duct configuration.

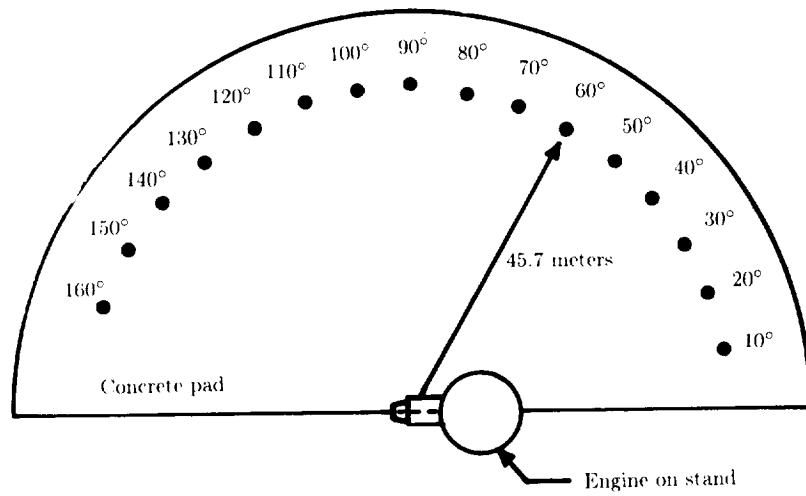


Figure 21. Test pad layout of full-scale engine test facility.

array of microphones. In the case shown, the microphone arc has a 45.7-meter radius, and a concrete pad between the engine and the microphones controls the conditions for the reflected wave.

One disadvantage of full-scale engine tests is the inability to separate the contributions from the various engine sources in the far-field measurement. The amount of suppression due to inlet treatment, for example, may be masked at certain radiation angles by the jet noise of the fan and core ducts. Several means of alleviating this problem have been proposed and investigated, including the use of barriers to shield inlet noise from exhaust noise and microphone arrays (or focusing mirrors) that focus on the noise being radiated from a particular region of space.

To obtain valid fan noise source levels representative of in-flight conditions, an "inlet turbulence control" structure, as shown in figure 22, is used. This eliminates some of the lower order modes generated by inflow distortion effects. When performing full-scale engine tests on the ground, one must choose between a bell-mouth-shaped inlet and a flight inlet. The bell-mouth inlet gives cleaner airflow with no forward motion of the engine, but changes the inlet geometry and therefore the directivity. The flight inlet gives poorer aerodynamic performance under static conditions, but has the proper geometry for duct termination radiation conditions.

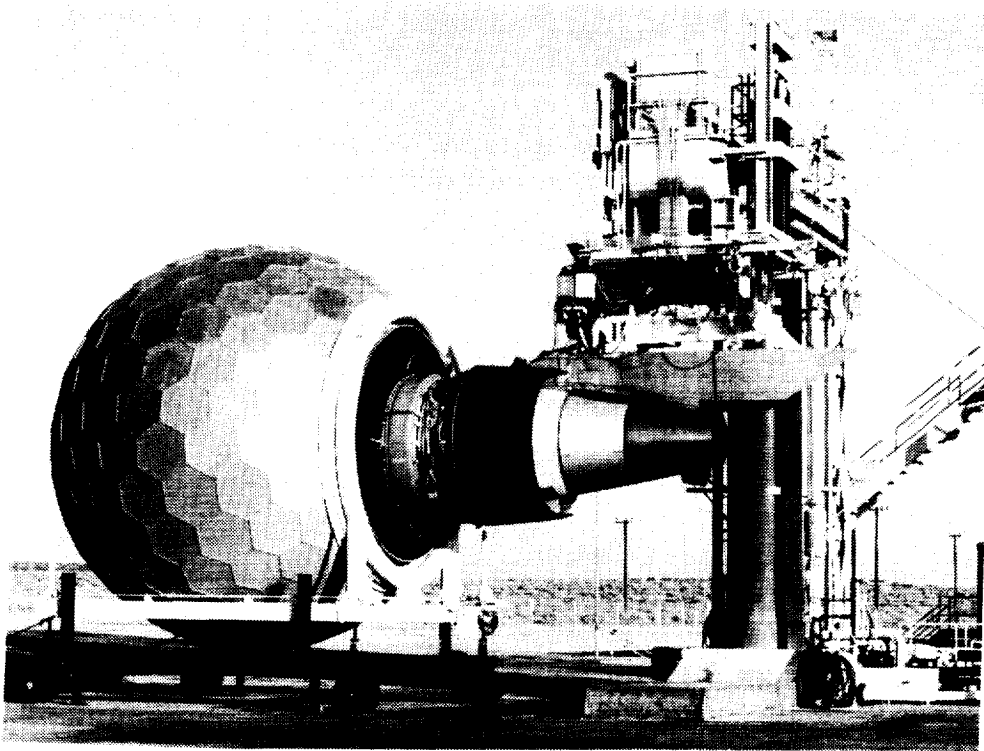


Figure 22. Full-scale engine test facility with turbulence control structure.

To measure the insertion loss of a treatment design in a full-scale inlet test, a prior test with a hard-walled inlet is necessary for comparison. Since full-scale engine

hardware and testing is so costly, this is often an unavailable luxury. Often, the most one might hope for is a comparison between the new design and the previously tested "standard" treatment design, so that the performance improvement might be determined.

Recommendations for Further Research

In the area of acoustic treatment impedance models, it has been suggested that a useful area of research might be the improvement of the impedance model for bulk absorber. Development of more practical and convenient methods to measure treatment panel impedance would be helpful.

Generally, further advancement in duct treatment design methods awaits improvements in theoretical prediction methods, either for duct propagation or turbomachinery source modal content. A useful area of innovation would be the development of more practical and efficient duct propagation prediction computer codes. Further work is needed in those areas where duct acoustics departs from ideal, axisymmetric conditions, such as ducts that are nonaxisymmetric or vary in cross-sectional area along the length of the duct. Propagation in nonuniform flow and the effects of boundary layers are important areas of research. Little research has been done into the effects of high sound pressure levels on propagation, a problem in nonlinear acoustics.

Despite the strong dependence on empirical or semiempirical methods, acoustic treatment design can be considered to be in a fairly advanced state of development. Current treatment designs are able to meet noise reduction certification requirements. Barring the possibility of a technology breakthrough, further increases in treatment effectiveness will provide marginal gains relative to development resources that must be applied. Impetus for this further research will come only if noise regulations change to the extent that new aircraft are no longer able to meet the certification requirements.

References

1. Beranek, Leo L., ed.: *Noise and Vibration Control*. McGraw-Hill Book Co., Inc., c.1971.
2. *Standard for Metric Practice*. ASTM Designation: E 380-85. Volume 14.02 of 1986 Annual Book of ASTM Standards, c.1986, pp. 339-380.
3. Groeneweg, John F.: Current Understanding of Helmholtz Resonator Arrays as Duct Boundary Conditions. *Basic Aerodynamic Noise Research*, Ira R. Schwartz, ed., NASA SP-207, 1969, pp. 357-368.
4. Kinsler, Lawrence E.; and Frey, Austin R.: *Fundamentals of Acoustics*, Second ed. John Wiley & Sons, Inc., c.1962.
5. Morse, Philip M.; and Ingard, K. Uno: *Theoretical Acoustics*. McGraw-Hill Book Co., Inc., c.1968.
6. Cremer, L.: *Theory of Attenuation of Airborne Sound in Rectangular Ducts With Absorbing Material on Their Inner Walls and the Resulting Maximum Attenuation*. BLL-NEL-TT-2590-(6075.461), British Library Lending Div., Boston Spa (England), 1973.
7. Zorumski, William E.; and Tester, Brian J.: *Prediction of the Acoustic Impedance of Duct Liners*. NASA TM X-73951, 1976.
8. Delany, M. E.; and Bazley, E. N.: Acoustical Properties of Fibrous Absorbent Materials. *Appl. Acoust.*, vol. 3, no. 2, Apr. 1970, pp. 105-116.
9. Hersh, A. S.; and Walker, B.: Acoustic Behavior of Fibrous Bulk Materials. AIAA-80-0986, June 1980.
10. Cole, Fred W.: Graphic Models for Acoustic Flow Resistance. Michigan Dynamics/AMBAC paper presented at the American Society for Metals 1969 Southern Metals Conference, Apr. 1969. (Available as Tech. Note MDD 503.)

11. Motsinger, R. E.; Syed, A. A.; and Manley, M. B.: The Measurement of the Steady Flow Resistance of Porous Materials. AIAA-83-0779, Apr. 1983.
12. Ingard, Uno: On the Theory and Design of Acoustic Resonators. *J. Acoust. Soc. America*, vol. 25, no. 6, Nov. 1953, pp. 1037-1061.
13. Kooi, J. W.; and Sarin, S. L.: An Experimental Study of the Acoustic Impedance of Helmholtz Resonator Arrays Under a Turbulent Boundary Layer. AIAA-81-1998, Oct. 1981.
14. Zandbergen, T.: On the Practical Use of a Three-Microphone Technique for In-Situ Acoustic Impedance Measurements on Double Layer Flow Duct Liners. AIAA-81-2000, Oct. 1981.
15. Rice, Edward J.: *A Theoretical Study of the Acoustic Impedance of Orifices in the Presence of a Steady Grazing Flow*. NASA TM X-71903, [1976].
16. Rice, Edward J.: *A Model for the Acoustic Impedance of a Perforated Plate Liner With Multiple Frequency Excitation*. NASA TM X-67950, 1971.
17. Rice, Edward J.: A Model for the Pressure Excitation Spectrum and Acoustic Impedance of Sound Absorbers in the Presence of Grazing Flow. AIAA Paper No. 73-995, Oct. 1973.
18. Bauer, A. B.; and Chapkis, R. L.: Noise Generated by Boundary-Layer Interaction With Perforated Acoustic Liners. *J. Aircr.*, vol. 14, no. 2, Feb. 1977, pp. 157-160.
19. Hersh, A. S.; and Walker, B.: The Acoustic Behavior of Helmholtz Resonators Exposed to High Speed Grazing Flows. AIAA Paper 76-536, July 1976.
20. Rice, Edward J.: *A Model for the Acoustic Impedance of Linear Suppressor Materials Bonded on Perforated Plate*. NASA TM-82716, 1981. (Available as AIAA-81-1999.)
21. Mechel, F.; Mertens, P.; and Schilz, W.: *Research on Sound Propagation in Sound-Absorbent Ducts With Superimposed Air Streams, Volumes I-IV*. AMRL-TDR-62-140, U.S. Air Force, 1962.
22. *Standard Test Method for Airflow Resistance of Acoustical Materials*. ASTM Designation: C 522-80. Volume 04.06 of 1986 Annual Book of ASTM Standards, c.1986, pp. 220-225.
23. *Standard Method of Test for Impedance and Absorption of Acoustical Materials by the Tube Method*. ASTM Designation: C 384-58. Part 14 of 1970 Annual Book of ASTM Standards, 1970, pp. 126-138.
24. Lippert, W. K. R.: The Practical Representation of Standing Waves in an Acoustic Impedance Tube. *Acustica*, vol. 3, no. 3, 1953, pp. 153-160.
25. Seybert, A. F.; and Ross, D. F.: Experimental Determination of Acoustic Properties Using a Two-Microphone Random-Excitation Technique. *J. Acoust. Soc. America*, vol. 61, no. 5, May 1977, pp. 1362-1370.
26. Fahy, F. J.: Rapid Method for the Measurement of Sample Acoustic Impedance in a Standing Wave Tube. *J. Sound & Vib.*, vol. 97, no. 1, Nov. 8, 1984, pp. 168-170.
27. Seybert, A. F.; and Parrott, T. L.: *Impedance Measurement Using a Two-Microphone, Random-Excitation Method*. NASA TM-78785, 1978.
28. Dean, P. D.: An In Situ Method of Wall Acoustic Impedance Measurement in Flow Ducts. *J. Sound & Vib.*, vol. 34, no. 1, May 8, 1974, pp. 97-130.
29. Rice, E. J.; and Sawdy, D. T.: *A Theoretical Approach to Sound Propagation and Radiation for Ducts With Suppressors*. NASA TM-82612, 1981.
30. Boyd, W. K.; Kempton, A. J.; and Morfey, C. L.: Ray-Theory Predictions of the Noise Radiated From Aeroengine Ducts. AIAA-84-2332, Oct. 1984.
31. Stimpert, D. L.; and McFalls, R. A.: *Demonstration of Short-Haul Aircraft Aft Noise Reduction Techniques on a Twenty Inch (50.8 cm) Diameter Fan*. NASA CR-134849, 1975.